Elsevier Editorial System(tm) for Geomorphology
Manuscript Draft

Manuscript Number:

Title: Automated mapping of glacial overdeepenings beneath contemporary ice sheets

Article Type: Research Paper

Keywords: Overdeepenings, automated landform mapping, glacial erosion, landscape evolution, Antarctica, Greenland.

Corresponding Author: Dr. Darrel Swift, PhD

Corresponding Author's Institution: University of Sheffield

First Author: Henry Patton

Order of Authors: Henry Patton; Darrel Swift, PhD; Chris D Clark; Stephen J Livingstone; Simon J Cook; Alun Hubbard

Abstract: Overdeepenings in the beds of glacial systems influence subglacial hydrology, ice flow dynamics, and ice-mass stability, yet a consensus regarding the mechanisms responsible for their formation is lacking. Fundamental data relating to overdeepening location and morphometry are urgently required to motivate process understanding of this phenomenon and to provide quantitative test-data for numerical ice-erosion models. Here, methods for mapping overdeepening distribution and extracting metrics relating to overdeepening morphology and topographic context are explored using subglacial topography datasets covering the whole of Antarctica and Greenland. Hydrological and terrain filtering approaches fail to capture complex overdeepening morphologies. A novel rule-based GIS methodology is therefore proposed that delineates overdeepening perimeters by analysing changes in closed-contour length with distance from initial points of elevation minima. A suite of quality-control criteria are also described that remove potentially spurious depressions typical of those created by interpolation in regions of sparse bed-elevation data. The ability to relate overdeepening characteristics to present ice-sheet characteristics means our approach provides significant potential to gain insight into critical subglacial processes that influence landscape evolution and ice sheet dynamics, as illustrated by the testing of a proposed relationship between overdeepening elongation ratio and ice sheet flow velocity. Improvements in the accuracy and resolution of bed-topography datasets, including novel methods that extrapolate empirical bed-elevation measurements using surface-ice velocities, will reduce the need for quality control procedures and facilitate increasingly robust insights from empirical data.

Suggested Reviewers: Matteo Spagnolo PhD
Senior Lecturer, School of Geoscience, University of Aberdeen
m.spagnolo@abdn.ac.uk
Dr Spagnolo has undertaken previous work on the analysis of glacial landform morphology using large datasets obtained by GIS/RS.

Chris Stokes PhD
Reader, Department of Geography, University of Durham
C.R.Stokes@durham.ac.uk

Dr Stokes has undertaken previous work on the analysis of glacial landform morphology using large datasets obtained by GIS/RS.

Christine Dow PhD
NASA Postdoctoral Fellow, Cryospheric Sciences Laboratory, NASA
christine.f.dow@nasa.gov
Dr Dow has undertaken previous research on ice-bed processes within overdeepenings beneath contemporary ice masses.

Kathryn Rose PhD
Postdoctoral Research Associate, School of Geographical Sciences, University of Bristol
k.c.rose@bristol.ac.uk
Dr Rose's research interests include ice sheet dynamics over diurnal to millennial time scales, long-term landscape evolution, glacial geomorphology, the linkages between large-scale glacial, fluvial and tectonic processes, and the application of geophysical techniques to glacial environments. Current work focuses on linking landscape form to glacial process and long-term landscape evolution in glacial environments.

The University Of Sheffield.

Department Of Geography.

The Editor
Geomorphology

01 August 2014

Head of Department
Professor Jean Grugel

Department of Geography
University of Sheffield
Winter Street
Sheffield S10 2TN
United Kingdom

Telephone: +44 114 222 7900
Fax: +44 114 222 7907
Email: d.a.swift@sheffield.ac.uk

Dear Sir

New manuscript submission *Automated mapping of glacial overdeepenings beneath contemporary ice sheets* by Patton, Swift, Clark, Livingstone, Cook and Hubbard

I hope that you will consider this submission for publication in the journal *Geomorphology*.

Amongst the glaciological and ice sheet modelling communities there is growing interest in the role of glacial landscape evolution and subglacial landforms in preconditioning and modulating ice sheet behaviour, particularly in relation to climate change. Of prime interest are **overdeepenings** – deep, glacially eroded bedrock depressions –that are major erosional landforms and are fundamental components of glaciated landscapes and ice sheet beds. Importantly, overdeepening of ice-sheet beds introduces reverse gradients that cause switches in subglacial drainage system morphology and promote instability during ice retreat. It is curious that subglacial erosion introduces major landforms into ice sheet beds that have potential to accelerate and destabilise ice flow, yet the processes that initiate overdeepenings and control their morphology remain poorly understood.

Our interest in this topic led to a substantial review paper in Earth-Science Reviews (Cook and Swift, 2012) that helped frame the importance of overdeepenings in ice sheet dynamics and highlighted the urgent need for quantitative data to improve understanding of the overdeepening process. **Our submitted manuscript describes a GIS-based mapping and landform analysis approach that has enabled us to obtain the first comprehensive quantitative dataset on overdeepening location and morphology for overdeepenings beneath the present ice sheets.** New methods of resolving ice sheet subglacial topography and the increasing sophistication of coupled numerical ice-sheet and landscape evolution models, which require quantitative data to validate model output, provide strong incentives for this approach. Using an example that explores the relationship between overdeepening elongation ratio and ice sheet velocity, our manuscript discusses the insights that can be gained from our approach and the potential limitations. Further exploration of our large dataset will be reported in a series of further manuscripts that are currently in preparation.

As corresponding author I would be pleased to answer any queries you may have in relation to this submission. My direct telephone number is 0114 222 7959.

Yours sincerely

Dr Darrel A Swift (corresponding author)
Lecturer in Geoscience

Highlights

Patton et al. Automated mapping of glacial overdeepenings beneath contemporary ice sheets.

- Overdeepenings are fundamental components of ice sheet beds
- We present methods for mapping overdeepenings and analysing overdeepening form
- Method offers potential to reveal relationships with present ice sheet parameters
- Overdeepening elongation ratio may reflect ice velocity
- Limitations of bed-topography datasets require strict quality control criteria

Automated mapping of glacial overdeepenings beneath contemporary ice sheets

Henry Patton[a,b,1], Darrel A. Swift[a,*], Chris D. Clark[a], Stephen J. Livingstone[a], Simon J. Cook[c], Alun Hubbard[b]

[a]*Department of Geography, University of Sheffield, Winter Street, Sheffield, S10 2TN, UK.*

[b]*Department of Geology, University of Tromsø – The Arctic University of Norway, N-9037 Tromsø, Norway.*

[c]*School of Science and the Environment, Manchester Metropolitan University, Chester Street, Manchester, M1 5GD, UK.*

[1]*Present address: Department of Geology, University of Tromsø – The Arctic University of Norway, N-9037 Tromsø, Norway.*

[*]*Corresponding author. Email d.a.swift@sheffield.ac.uk. Telephone +44 114 222 7959.*

ABSTRACT Overdeepenings in the beds of glacial systems influence subglacial hydrology, ice flow dynamics, and ice-mass stability, yet a consensus regarding the mechanisms responsible for their formation is lacking. Fundamental data relating to overdeepening location and morphometry are urgently required to motivate process understanding of this phenomenon and to provide quantitative test-data for numerical ice-erosion models. Here, methods for mapping overdeepening distribution and extracting metrics relating to overdeepening morphology and topographic context are explored using subglacial topography datasets covering the whole of Antarctica and Greenland. Hydrological and terrain filtering approaches fail to capture complex overdeepening morphologies. A novel rule-based GIS methodology is therefore proposed that delineates overdeepening perimeters by analysing changes in closed-contour length with distance from initial points of elevation minima. A suite of quality-control criteria are also described that remove potentially spurious depressions typical of those created by interpolation in regions of sparse bed-elevation data. The ability to relate overdeepening characteristics to present ice-sheet characteristics means our approach provides significant potential to gain insight into critical subglacial processes that influence landscape evolution and ice sheet dynamics, as illustrated by the testing of a proposed relationship between overdeepening elongation ratio and ice sheet flow velocity. Improvements in the accuracy and resolution of bed-topography datasets, including novel methods that extrapolate empirical bed-elevation measurements using surface-ice velocities, will reduce the need for quality control procedures and facilitate increasingly robust insights from empirical data.

Keywords: overdeepenings, automated landform mapping, glacial erosion, landscape evolution, Antarctica, Greenland.

1. Introduction & aims

The mechanisms by which glaciers and ice sheets form spectacular alpine and fjord landscapes are well known, and such landscapes have been exploited widely for purposes of palaeo-glaciology and process understanding (e.g. Glasser and Bennett, 2004). Recently, this understanding has been aided by implementation of simple ice-erosion laws within numerical models, which are able to simulate depths and patterns of glacial incision with compelling success (e.g. Kessler et al., 2008). However, the mechanisms that produce overdeepenings (Fig. 1A–B) remain unclear, and the implementation of candidate processes within ice-erosion models has met with limited success (e.g. Egholm et al., 2012).

The reverse-bed gradient that occurs in the presence of an overdeepening has been shown to exert strong influence on glacier hydrology, ice dynamics, and ice-mass stability (e.g. Schoof, 2007; Cook and Swift, 2012; Stokes et al., 2014) (cf. Fig. 1C), meaning a complete understanding of overdeepening form and origin is essential to elucidate and understand critical ice-bed processes and to inform predictions of past and present ice-mass behaviour. Cook and Swift (2012) have argued that process understanding has been disadvantaged by an absence of quantitative studies of overdeepening morphology that perhaps reflects the term's uncertain etymology and, as a possible consequence, an unconscious disregard of overdeepenings as distinct morphological features. Hence, fundamental data are urgently required to motivate process understanding in this arena, as well as to provide quantitative test-data for ice-erosion models.

In this paper, we develop a computationally efficient GIS-based methodology for mapping of overdeepenings and quantification of their morphometry. Following similar studies that have investigated glaciological depositional phenomena (e.g. Clark et al., 2009; Stokes et al., 2013), we develop methods that can be used to extract overdeepening length, width, depth and volume, as well as overdeepening long- and cross-profiles showing that pass through the deepest point. Measurements of these phenomena require delimitation of the basin perimeter and identification of basin in- and out-flow points, and also require identification of nested overdeepenings (e.g. Fig. 1C–D). From these measurements, metrics such as elongation ratio (cf. Clark et al., 2009), normal and adverse slope lengths and gradients, and planform area can then be derived (Fig. 2).

We use comprehensive subglacial topography datasets for the Antarctic and Greenland ice sheets (Bamber et al., 2013; Fretwell et al., 2013) to illustrate a possible application of our methodology that seeks to relate overdeepening form to ice velocity. These recently published datasets provide an incentive for the development of landscape analysis tools that enable systematic analysis of ice-sheet beds, not least because the application of traditional methods of geomorphological mapping at this scale is inappropriate. Nevertheless, automated analysis of such datasets raises problems

associated with dataset quality and resolution, the presence of features of non-glacial origin, and the inherently different timescales of ice mass and landscape response. In addition, we find that insights are limited by the quality of the metrics that present data permit.

2. Study areas and datasets

2.1 Study areas

The landscape beneath present-day ice sheets provides an unparalleled opportunity to elucidate ice-bed processes and evolution because of the size of the ice-covered area and, where ice cover remains present, the absence of postglacial deposits that in palaeo-glaciated landscapes accumulate in areas of low-elevation. Comprehensive subglacial topography datasets for the Antarctic (Bedmap2) and Greenland ice sheets have recently been made available (Bamber et al., 2013; Fretwell et al., 2013) and these are used in the example application of our methods in section 5. For practical purposes, the development of these methods was undertaken on a relatively small domain surrounding the Byrd Glacier catchment and Transantarctic Mountains, adjacent to the Ross Ice Shelf, in East Antarctica (Fig. 3). This 5.22×10^5 km^2 region provides an excellent methodological test-bed, combining substantial variability in relief with the presence of a large number of bed depressions that exhibit a range of depths and areas.

2.2 Antarctic subglacial topography

The Bedmap2 dataset provides subglacial and continental shelf topography for the Antarctic continent (Fretwell et al., 2013) using the most up-to-date compilation of empirical ice-thickness measurements for the Antarctic ice sheets. Raw ice-thickness data for Bedmap2 have been derived from a variety of sources, including: direct airborne radar sounding and seismic measurements; satellite altimetry and free-air gravity surveys; and 'synthetic' data computed using a 'thin-ice' model. The rationale for including modelled topography within the source data was to prevent rock outcrops from overly skewing the ice-thickness distribution in mountainous areas where few empirical measurements exist. Although this output gives the appearance of accurate relief within ice-marginal mountain ranges, it is worth noting that this topography is not directly constrained by any empirical data. Continental shelf topography is derived from the GEBCO 2008 bathymetric compilation mosaiced with sub-ice shelf data from Timmermann et al. (2010).

The Bedmap2 topography is rendered on a 1-km grid but empirical and synthetic measurements of ice thickness were sampled at 5 km, primarily because the distribution of empirical measurements, which require interpolation (kriging) to form a continuous surface, did not warrant a higher resolution (Fretwell et al., 2013). Notably, the highly anisotropic distribution of ice-thickness measurements obtained by airborne radar surveys, in which across-track sampling density is

potentially 3 or 4 orders of magnitude lower than the density along the flight tracks, means that even large, valley-scale features may be absent or resolved poorly. Furthermore, the fragmentary nature of completed radar surveys carried out across Antarctica has left many regions sparsely constrained. For example, in Bedmap2, 80% of grid cells have data within 20 km, and the greatest distance from a grid cell to the nearest data point (the 'poles of ignorance') is ~ 230 km (Fretwell et al., 2013). For this reason, the non-genetic term *bed depression* is used when describing the methodological aspects of this study, thereby avoiding the implication that all basin-like features in the DEM surface are genuine enclosed-depressions and/or glacial overdeepenings.

2.3 Greenland subglacial topography

Subglacial and continental shelf topography for Greenland is provided by Bamber et al. (2013). As with Bedmap2, topography in this dataset is rendered on a 1 km grid with subglacial topography mainly derived using ice-thickness measurements obtained from airborne radar surveys and satellite observations. As such, similar error sources, assumptions and levels of uncertainty exist. Continental shelf topography is sourced from the most recent IBCAO (International Bathymetric Chart of the Arctic Ocean) compilation of offshore bathymetric datasets (Jakobsson et al., 2012), supplemented with additional soundings from Jakobshavn fjord. It should be noted that where bathymetry is not well known, or observations do not exist, bed elevations are often underestimated by up to several hundred metres, particularly within fjordal zones (Bamber et al., 2013).

2.4 Additional datasets

Higher-resolution ice thickness datasets for several areas of Antarctica were obtained from the Centre for Remote Sensing of Ice Sheets archive (CReSIS; https://data.cresis.ku.edu) for evaluation of the Bedmap2 mapping results, especially the implications of Bedmap2 resolution for delineation of overdeepening perimeters. These products, which have restricted geographical coverage, are derived from airborne radar surveys and are published at a grid spacing of 500 m. Ice-surface velocity data derived from InSAR observations over Antarctica and Greenland were sourced from datasets compiled by Rignot et al. (2011a) and Joughin et al. (2010a) respectively.

3. Automated mapping of overdeepenings

3.1 Delimitation of overdeepenings in the landscape

A key challenge in mapping geomorphological phenomena is delineating their boundaries. For example, overdeepenings do not represent isolated pockets of deep glacial erosion in an otherwise unmodified fluvial landscape. Most frequently, overdeepenings occur as areas of slightly deeper

133 erosion in the profile of deep, glacially-carved valleys (cf. Cook and Swift, 2012), and as such the
134 flanks of an overdeepened basin are inseparable from those of the host valley. Further, for
135 subglacial phenomena, landform context is influenced by the presence of overlying ice. For
136 example, subaerial and subglacial hydraulic gradients will differ, meaning that an overdeepening
137 in the subaerial environment which forms a closed basin and therefore contains a lake will only
138 contain a subglacial lake (assuming the lake is overridden by ice) if the gradient of the adverse
139 bed-slope exceeds 11 times that of the ice-surface gradient (cf. Clarke, 2005). Further, the
140 'surface' of the subglacial lake will be inclined in the opposite direction to ice flow, and the
141 gradient of the subglacial lake 'surface' will vary in response to changes in ice-surface and
142 hydraulic gradients during glacial advance and retreat.

143 For the purpose of this study, we follow Cook and Swift (2012), who use *overdeepening* (verb) to
144 describe the excavation of a bedrock depression that, in a subglacial context, would require ice,
145 water and sediment to traverse a locally reversed (or adverse) slope. This usage therefore describes
146 the creation of a specific landform, an *overdeepening* (noun), which on deglaciation would form a
147 sedimentary basin or lake (cf. Fountain and Walder, 1998). This definition of an overdeepening as
148 a subaerial enclosed depression means that the elevation at the outflow point can be used to
149 delineate the depression perimeter. Mapping of enclosed depressions in predicted subglacial
150 hydraulic potentials (cf. Shreve, 1972) is avoided intentionally because depression form and
151 location would depend partly on the morphology of the ice surface, which is inherently variable. A
152 classification based on purely morphological grounds is therefore independent of glaciological
153 processes. Clearly, enclosed-depressions can also be formed by non-glacial processes, including
154 tectonic processes (e.g. by faulting), whilst some are artefact depressions that have no basis in
155 reality (see above). Methods of identifying erroneous depressions and tectonic basins are also
156 therefore considered in this study.

157 Despite the morphological simplicity of enclosed-depressions, mapping methodology must
158 overcome several important challenges. Firstly, automated analyses of digital elevation models
159 (DEMs) at the ice-sheet scale, even at 1 km resolution, require computationally efficient
160 techniques. Secondly, like other bedforms (cf. Clark et al., 2009), overdeepenings tend to develop
161 a distinctive ovoid planform regardless of size (Cook and Swift, 2012), but constraints imposed by
162 topography often produce sinuous overdeepenings that follow the axes of large troughs (e.g. Fig.
163 1B), while others are influenced by geological structures or changing phases of ice-flow direction,
164 resulting in circular or irregular shapes. Thirdly, overdeepenings are frequently nested (cf. Fig.
165 1D), with larger examples occasionally containing many generations of nesting. Finally, many
166 overdeepenings beneath contemporary ice sheets may be relict landforms that represent erosion
167 during earlier stages of glaciation, which may limit meaningful analysis of mapping results. For

example, ice flow direction during depression formation, and thus the location of in- and out-flow points, cannot always be established.

3.2 Delineation methods

This section evaluates three GIS-based methodologies for delineating depressions in a DEM surface that would constitute subaerial close-basins in a landscape. The third approach has been adopted for this study.

3.2.1 Hydrological filling

In the post-glacial landscape, overdeepenings are sinks for water and sediment (e.g. Preusser et al., 2010; van Rensbergen et al., 1999). An intuitive approach to mapping overdeepenings therefore takes advantage of hydrological GIS tools to identify sinks (or areas of internal drainage) across the digital terrain (e.g. Arnold, 2010). 'Fill' tools offer the simplest approach, and work by filling sinks iteratively until each has reached its capacity, thereby creating a 'depressionless' DEM. A major disadvantage when applied on the scale of whole continents is that very large areas of the landscape become filled that are in fact tectonic basins or rift systems, meaning many smaller nested depressions that may be glaciological in origin remain unrecognised (Fig. 3).

3.2.2 Terrain filtering

A more sophisticated yet computationally simple approach to mapping overdeepenings is to apply signal-processing techniques to the DEM surface (e.g. Leonowicz et al., 2009; Stumpf et al., 2013). This approach considers the landscape as a three-dimensional waveform within which depressions and mountain peaks represent anomalous interference. By filtering the elevation data at specific wavelengths, a smoothed surface largely voided of relief (interference) can be created. Overdeepened topography can then be extracted by calculating the negative residuals beyond a given threshold compared to its original form. Figure 4 shows how a two-dimensional, circular (200 km), low-pass Gaussian filter of the form

$$f(x,y)=(1/2\pi\sigma^2)e^{-[(x-\mu_x)^2+(y-\mu_y)^2]/(2\sigma^2)}, \quad (1)$$

where sigma (σ) and mu (μ) are the standard deviation and mean of the elevation distribution respectively, can be used to produce a map of potential areas of overdeepening. In contrast to basin extents mapped using hydrological filling techniques (above), this approach lacks precise thresholds required for delimiting closed depressions. Furthermore, the approach does not indicate an intuitive automated mechanism for mapping nested features. A more rigorous GIS-based

198 approach is therefore needed that can systematically differentiate the complex relief of large
199 depressions.

200 ***3.2.3 Contour tracking***

201 A final approach to delineating overdeepenings is to track changes in closed-contour length as an
202 observer moves away from an elevation minimum. The mapping process is threefold. Firstly, a
203 terrain analysis mask was calculated that delimits depression-like areas in the DEM surface (Fig.
204 5A–B). By eliminating large areas of the surface that are not depression-like, this initial step
205 greatly enhances computational efficiency at the continental scale. Secondly, locations of elevation
206 minima were pinpointed using zonal statistical analyses to find the minimum point within each
207 closed-contour that intersected the terrain-analysis mask. (Fig. 5C). Finally, changes in contour
208 length are tracked to identify a sudden increase in length, indicating that the contour in question is
209 above the elevation of the contour defining the enclosed depression (Fig. 6A). Steps one and three
210 were implemented as follows using toolboxes and algorithms found within ArcGIS 10.1 and
211 GRASS GIS, with automated workflow achieved using packages within Python such as ArcPy.
212 Where methods contain free parameters, values have been chosen that provide sensible results, but
213 these are far from definitive.

214 *3.2.3.1 Terrain analysis mask*

215 Many existing methods of automated terrain analyses have their roots in differential geometry,
216 using combinations of morphometric parameters such as slope, gradient, curvature and aspect to
217 classify the form of the DEM surface (e.g. Evans, 1980; Wood, 1996; MacMillan et al., 2000;
218 Wilson and Gallant, 2000; Drăguţ and Blaschke, 2006; Klingseisen et al., 2008; Brenning, 2009;
219 Saha et al., 2011). Here, two parameters are used to delimit a broad areas of depression-like relief:
220 plan curvature (horizontal curvature, intersecting with the XY plane) and minimum curvature in
221 the direction perpendicular to the direction of maximum curvature. The quantitative foundation to
222 this methodology thus creates several free parameters, the sensitivity of which can be fine-tuned
223 depending on the desired mapping criteria. For example, plan convexity and minimum curvature
224 can be tuned to mask only small cirque-like features that are confined by high topography.

225 *3.2.3.2 Contour analysis*

226 Depression perimeters were delineated by determining the highest elevation 'bounding contour'
227 using a 'contour-tracking' algorithm. This monitors the length change between successive
228 contours intersected by a linear transect drawn from each elevation minima (Fig. 6A). A
229 depression was considered to have been 'breached' at the first contour to demonstrate a length
230 90% longer than the preceding contour, indicating that the preceding contour bounded the
231 depression perimeter. This threshold length increase represents a factor-of-three increase in the

bounded area. The algorithm was used to identify generations of nested depressions (Fig. 6B) by running multiple passes whilst 'ignoring' previously identified depression breaches. Ordering of the parent and child depressions was classified based on simple relative positioning, using a top-down approach (Fig. 6C).

3.2.3.3 Dataset filtering

At this stage in the contour tracking approach, additional parameters can be used to filter the dataset of mapped depressions and thereby facilitate further dataset analysis:

- Minimum perimeter: this parameter can be set to exclude very small depressions that may be artefacts created by interpolation algorithms used in the creation of the DEM.

- Maximum perimeter: this parameter can be set to exclude very large depressions (e.g. tectonic basins, plateaus).

- Maximum transect: the length of the transect used for tracking changes in contour length can be set to exclude very large depressions (e.g. tectonic basins, basin-shaped plateaus).

4. Automated extraction of overdeepening metrics

Whilst mapping methods (above) can provide qualitative information on the distribution, planform morphology and nesting of potential overdeepenings, further methods are required to extract quantitative measurements of overdeepening form (e.g. Fig. 2). GIS-based methods suitable for extracting such metrics from very large numbers of mapped overdeepenings are described below.

4.1 Depression in- and out-flow points

The identification of depression entry and exit points is a critical step in the measurement and analysis of depression length and of long-profiles that approximate the flow-paths of ice and subglacial water and sediment. In order to provide adaptability to different contexts, three approaches are presented here: two that utilise the bed topography alone, which may be appropriate where ice-cover data are not available (e.g. palaeo domains), and one that uses ice-surface elevation data, which is the method chosen for this study. All three approaches have methodological limitations, a summary of which is given in Table 1. In addition, changes in ice-flow direction and water and sediment routing over time mean that in- and out-flow points relevant at the time of overdeepening formation cannot be known.

4.1.1 Topography based

Where grounded ice-thickness data do not exist (e.g. continental shelves and palaeo ice-sheet domains), in- and out-flow points can be inferred by identifying broad trends in landscape elevation by means similar to the filtering methodology presented in Section 3.2.2. However, thick ice sheets may become independent of topography and may subsume and dissect mountain ranges, meaning ice-flow directions can reverse as ice sheets grow. For the Byrd test domain, a 1500 km^2 moving window is required to identify a general trend in relief that is sufficient to overcome the influence of the Transantarctic Mountains against the more general westwards flow of the East Antarctic Ice Sheet. By reducing the size of this moving window, more localised trends in elevation change can be extracted, which may be suitable for defining in- and out-flow points during periods when glaciation was more restricted and smaller ice masses occupied only higher elevations. However, different sectors of a single ice sheet can be characterised by contrasting styles of glaciation, meaning this method can be difficult to apply across ice-sheet scale domains.

4.1.2 Hydrology based

An intuitive approach to identifying in- and out-flow points where ice-thickness data are absent is to use 'hydrological tools' to calculate flow direction and flow accumulation rasters for the DEM surface. These can be used to identify locations where maximum flux both enters and leaves each depression. However, the assumption that subaerial flow represents an accurate proxy for ice flow does not hold true for ice sheets, especially where ice sheet flow is independent of the underlying topography. If ice thickness is known, a more robust approach would be to model the subglacial flow network by calculating hydraulic potentials (cf. Shreve, 1972) at the ice-bed interface. Nevertheless, subglacial water flow patterns can be subtly independent of ice flow, and may be unstable even under small changes in ice-surface gradient or ice-mass extent.

4.1.3 Ice-surface based

The preferred method for identifying in- and out-flow points in this study uses the elevation of the overlying ice-sheet surface. Assuming that the surface of ice flowing immediately above an overdeepening approximates a uniform plane that slopes in the direction of flow, the points of maximum and minimum ice-surface elevation that lie above the bounding contour of the depression (Fig. 7) will provide a reasonable approximation for the principal entry and exit points in terms of the greatest flux of ice. Where multiple points of equal ice-surface elevation exist around the depression edge, a single in- or out-flow point can be determined by choosing the point most distant from the basin minima. The suitability of this method collapses under relatively flat ice surfaces such as those of ice shelves, and where overdeepening planform is highly complex.

However, application to the test area domain (Fig. 8) demonstrates that this method is robust in most contexts.

4.2 Depression profiles and metrics

Following the identification of depression minima, bounding contours and in- and out-flow points, a range of descriptive profiles and quantitative metrics can be extracted for each depression (e.g. Fig. 2). Many of the metrics are readily calculated using simple GIS techniques and to give a thorough description here would be unnecessary. However, some, such as the long-profile and the calculation of elongation ratio for sinuous or asymmetric depressions, require bespoke methods.

4.2.1 Long-profiles

For depressions with sinuous planforms, the path of a long profile that follows the deepest route through the depression is far removed from a straight line that joins the in- and out-flow points. A convenient solution is to calculate a 'least-cost' path between the in-flow and out-flow points, with the resulting paths joining at the depression minimum (Fig. 8B). For adverse slopes with gradients that are below 11 times the ice surface gradient (cf. Clarke, 2005), this path will approximate the route taken by subglacial water through the depression. It is recognised, however, that patterns of subglacial water flow will also change as the ice mass waxes and wanes, meaning that flow patterns predicted by the contemporary ice-sheet surface may not reflect those prevalent during the time of overdeepening formation. Consequently, more complex hydrological methods for determining the depression long-profile were deemed to be unwarranted.

4.2.2 Depression shape

The shape of each mapped feature can provide important information on its probable origin and history of erosion. For example, depressions that conform most closely to a 'classic' ovoid shape may be considered more likely to have a glacial origin than those with a complex shape, and a glacial origin may be considered even more secure for those ovoid depressions that are elongate in the direction of present ice flow. Small, isolated and circular depressions are characteristic of artefact depressions created by kriging at flightline intersections in regions of sparse empirical data, which give rise to a 'pockmarked' DEM surface.

Three shapes are thus of interest: circular, elongated, or complex (unclassified). Absence of elongation can be assessed using a minimum bounding geometry methodology, whereby a depression is enclosed within a polygon that is defined by its minimum possible area (Fig. 9A). Where a depression fills more than 60% of a square polygon, it can be classified as 'circular'. However, elongation cannot be assessed using this method if a depression exhibits strong sinuosity (e.g. Fig. 1B) or a complex planform. As a result, we refine the concept of elongation such that

elongation is determined with respect to the presumed direction of ice-flow at all points along the depression long-profile. This can be achieved by calculating the mean width of the depression perpendicular to the least-cost transect between the in-flow and out-flow points (Fig. 9B). Using this method, we define elongated depressions to be those where the elongation ratio (transect length divided by mean width) exceeds 2. Depressions that exhibit neither circularity nor elongation in the direction of ice flow are deemed 'unclassified'.

4.3 Contextual classification

Overdeepening form and location is likely to be influenced by a range of local factors that affect erosion potential, including lithological changes or weaknesses and the location of moulins that direct surface runoff to the glacier bed (Hooke, 1991; Herman et al., 2011; Cook and Swift, 2012). Often, the simplest method for isolating such external drivers will be by cross-referencing depression location and/or relevant metrics with other numerically modelled or empirical datasets. Other factors can be isolated by automated classification of mapped depressions using such datasets. For example, empirical observations have indicated that topographic-focussing of ice flux in regions of high relief is a strong control on overdeepening location and depth (e.g. Kessler et al., 2008; Roberts et al., 2010). In this instance, a depression can be classified as 'topographically confined' using a simple proximity-based GIS-method that calculates the mean elevation of the topography within a small (20 km) buffer of the depression perimeter.

5. Applications of overdeepening metrics: assessment of the influence of overriding ice velocity on overdeepening morphology

The methods outlined above enable acquisition of data on overdeepening morphology for statistically large samples. For example, application of these methods to the subglacial topography datasets for Antarctica and Greenland (Bamber et al., 2013; Fretwell et al., 2013; Patton et al. in prep) results in a database of 13,000+ bed depressions (including nested depressions). To demonstrate the potential insight that can be gained from such datasets, we explore the relationship between overriding ice velocity and overdeepening morphology. We nevertheless acknowledge important uncertainties associated with current subglacial topography datasets and apply strict quality-control criteria to our mapping of bed depressions and analyses of their metrics. We anticipate that future improvements to such datasets will, in time, obviate the need for such restrictive criteria.

5.1 Subglacial topography uncertainties and quality-control procedures

Comparison of mapping results for Bedmap2 and for the higher-resolution CReSIS dataset (Fig. 10) demonstrates that the anisotropic distribution of empirical measurements in both datasets

359 produce artefacts that are mapped as bed depressions. In the Bedmap2 topography, these artefacts
360 mainly constitute smaller, isolated, spherical depressions that are aligned with the flightlines used
361 to collect airborne radar measurements of ice thickness (Fig. 10C). Mapping of the same domain
362 from the higher-resolution dataset identifies a significantly greater number of bed depressions,
363 many of which have a similar isolated, spherical appearance, albeit at a smaller scale
364 commensurate with the increased resolution of the dataset and density of flightlines (Fig. 10D). In
365 contrast, the first-order characteristics of larger depressions do not differ substantially when
366 mapped using the higher-resolution dataset, as demonstrated by planform (Fig. 10C–D) and long-
367 profile (Fig. 10E) characteristics of the Byrd Glacier depression. Mapping from higher-resolution
368 datasets therefore improves the detail in respect of the outlines of larger and some smaller
369 depressions and the metrics for some smaller depressions, artefact depressions are still present.
370 Consequently, to avoid the inclusion of spurious metrics from artefact depressions, mapping of
371 overdeepenings from gridded datasets requires application of quality control criteria regardless of
372 data resolution.

373 For this study, a suite of benchmark criteria relevant to ice sheet subglacial topography datasets
374 (Bamber et al., 2013; Fretwell et al., 2013) have been defined that are based on known
375 methodological and instrumental uncertainties (cf. section 2.2):

376 1. Bed-elevation uncertainty. Absolute bed-uncertainty data beneath grounded ice is provided
377 with the DEMs for Greenland and Antarctica (Fretwell, et al., 2013; Bamber et al, 2013).
378 Although this is a good measure for estimating uncertainties in overdeepening absolute depth
379 (i.e. the elevation of the deepest point in relation to sea level), it is not a robust criterion for
380 assessing adequate delineation of mapped features, which is dependent on relative
381 uncertainties in the immediate area of the bed. For this reason, criteria based on flightline
382 density and depression size (below) were also considered.

383 2. Flightline density. Criteria were used to specify a minimum depression width in regions of
384 sparse empirical data, resulting in the removal of small, isolated depressions characteristic of
385 artefact depressions produced by kriging. Areas of sparse data were identified using a
386 flightline density mask that showed the density of flightlines within a 10 km radius of each
387 grid cell. Depressions with widths less than 20 km were excluded if they did not intersect areas
388 with densities > 0.11, which is roughly equivalent to two flightlines within the given radius.
389 The choice of criteria reflects the observation by Fretwell et al. (2013) that absolute errors in
390 elevation generally increase over distances of up to 20 km, beyond which errors appear largely
391 uncorrelated with distance.

3. Depression size. Several size criteria were employed. Firstly, large features (e.g. tectonic basins) were removed by excluding depressions with bounding contours exceeding 2,000 km in perimeter (an area equivalent to 1.5 times the catchment area of Pine Island Glacier, Antarctica; cf. Vaughan et al., 2006). Depressions beyond this size are unlikely to have a glacial origin. Secondly, in regions with flightline densities > 0.11, depressions with adverse slopes shorter than 5 km were excluded because depressions of this size were unlikely to be adequately resolved by empirical measurements. Finally, a minimum overdeepening depth of 40 m was applied regardless of other criteria because shallow depressions are likely to have many sources, including kriging, bed elevation uncertainty, and geology. This value is intermediate between the minimum published absolute uncertainty values for the Bedmap2 (±66 m) and Greenland (±10 m) datasets (Fretwell, et al., 2013; Bamber et al, 2013).

4. Elongation with respect to the current ice-flow direction (cf. section 4.2.2). In accordance with the majority of landforms sculpted by flowing ice (e.g. flutes, drumlins, roche moutonnées, troughs), overdeepenings are generally elongate in the direction of ice flow. This criteria can therefore be applied to exclude potentially non-glacial depressions. Though some genuine overdeepenings will be excluded, including those with complex planforms formed under previous ice-flow configurations, strict filtering of landforms on the basis of ice flow direction will be beneficial for many applications because it should remove 'relict' landforms or those with complex morphologies that are unlikely to be in equilibrium with present ice sheet processes.

5. Topographic confinement. Observations indicate that overdeepenings are most common where ice flow is topographically confined (e.g. within valleys and outlet glacier troughs). When applied in conjunction with (4), this criteria can be used to further exclude potentially non-glacial depressions and, because ice flow within troughs must respect the trough axis, depressions where it is conceivable that morphology may have been inherited from ulterior flow directions under previous ice-flow configurations. Depressions were classified as topographically confined if the mean elevation of topography surrounding the depression exceeded the elevation of the lip by greater than 500 m (cf. section 4.3; Fig. 9C).

5.2 Influence of overriding ice velocity on overdeepening morphology

It is now accepted widely that many glacially moulded bedforms, including flutes, drumlins and mega-scale lineations lie on a continuum of scale that reflects the velocity of overriding ice (e.g. Clark et al., 2009; Heidenreich, 1964; Stokes and Clark, 2002). The elongation ratio (ER) in particular is assumed to correlate strongly with ice velocity for these phenomena, with analysis of high landform ER values often used to infer ice-streaming conditions (e.g. Clark, 1993; King et al.,

2009; Ó Cofaigh et al., 2013; Stokes and Clark, 1999). A similar correlation may exist for overdeepenings because fast-flowing ice should enhance rates of headward erosion by quarrying and abrasion (Herman et al., 2011; cf. Hooke, 1991) and rates of sediment evacuation and abrasion at the overdeepening lip (cf. Alley et al., 2003). Proof of this relationship would have significant value for palaeoglaciological research because it would provide information on former ice velocities in regions where erosional processes have dominated or the preservation of depositional bedforms has been poor. Importantly, subglacial topography datasets for the present ice sheets enable testing of such relationships with a level of confidence that was previously unattainable because overdeepenings in formerly glaciated contexts are obscured by postglacial sedimentation and data on former ice sheet velocities provided by numerical models is poorly constrained.

To test the relationship between overdeepening ER and ice velocity for contemporary ice sheets, our mapping methods allow the ER of Greenland and Antarctic depressions to be plotted against surface-ice velocities (Joughin et al., 2010b; Rignot et al., 2011b) measured above the deepest point in each depression (Figure 11). Because of dataset limitations and uncertainties regarding the origin and morphological inheritance of nested depressions, we restrict our analysis to 'parent' depressions that are elongated in the direction of ice flow and that pass the other quality criteria detailed above. In addition, we analyse separately the subset of depressions that can be categorised as 'topographically confined'. Not unexpectedly, these plots show substantial scatter that is consistent with the limitations of the source datasets and the simplicity of our approach. For example, scatter will be introduced by changes in ice sheet configuration that mean measured ice velocity is not necessarily indicative of mean ice velocity over the timescale of overdeepening formation, whilst overdeepening width is likely to be limited by valley width, such that valley width will also influence the elongation ratio. In addition, reverse slopes have been observed to promote ice-bed decoupling (cf. Alley et al., 2003) and to exert backstresses on ice flow (cf. Nick et al., 2009), meaning processes associated with overdeepenings may promote or resist ice flow according to the specific morphology of the adverse slope (cf. Cook and Swift, 2012). Nevertheless, Figure 11 does indicate potential relationships between ER and velocity, and it is apparent that overdeepenings are largely absent in regions where ice velocities fall below ~ 10 m a^{-1}. Furthermore, relationship significance is strongest for the subset of topographically confined depressions, which excludes depressions for which it is conceivable that the legacy of erosion under unknown, previous ice-flow directions has affected depression ER. The application of strict quality criteria means that the inclusion of spurious depressions arising from DEM artefacts is not thought to be a significant influence on the observed relationships.

6. Discussion

6.1 Identification and analysis of overdeepenings

The compilation of glacial-landform datasets alongside improvements in the resolution of remotely sensed data has led to numerous and detailed analyses of subglacial phenomena across palaeo-glaciated domains, including drumlins (Clark et al., 2009), glacial lineations (Greenwood and Clark, 2009; Spagnolo et al., 2014; Stokes et al., 2013), meltwater channels (Margold et al., 2011) and ribbed moraine (Dunlop and Clark, 2006). Much of this work has been driven by the need to decipher the glaciological significance of such landforms, as well as the need to obtain robust data to enable testing of numerical models that simulate ice sheet and landscape evolution processes (e.g. Evans, 2009; Jamieson et al., 2010; Melanson et al., 2013). Given the strong influence exerted by reverse bed slopes on subglacial hydrology, ice-flow dynamics and ice-sheet stability, the acquisition of similar data for understanding of overdeepening form and evolution is important. In addition, it is important that relevant communities, specifically geomorphologists, glaciologists and numerical modellers, work together to identify real and simulated landscape features that can be exploited for model testing and to expedite process understanding. Overdeepenings are a key landform in this respect because of the lack of consensus on their origin and their far-reaching influence on critical ice-bed processes and ice-sheet behaviour (cf. Cook and Swift, 2012).

The publication of relatively high-resolution bed-topography datasets covering the entire Antarctic and Greenland ice sheets has provided a major opportunity to advance our understanding of the evolution of subglacial landscapes and, importantly, the co-evolution of ice sheets, landforms and subglacial processes. These datasets avoid the disadvantage of post-glacial infilling and burying of erosional features that complicate analyses of overdeepenings and similar features, e.g. tunnel valleys, in palaeo-domains (Huuse, 2000; Hansen et al., 2009; Preusser et al., 2010; Moreau and Huuse, 2014). In addition, the present ice sheets have remained largely stable features for much of the recent geological past (e.g. Huybrechts, 1993), meaning landscapes and landforms shaped by characteristically slow subglacial processes, and the ice sheets themselves, are more likely to have achieved equilibrium forms that are in balance with climatic, glaciological and tectonic forces. Furthermore, the ability to correlate subglacial landform morphology and location with ice sheet characteristics obtained by measurement of present ice sheet parameters, including velocity and thermal regime, is unprecedented. Novel approaches that use surface ice motion to extrapolate sparse ice thickness measurements to larger areas with few or no data (e.g. Morlighem et al., 2014) promise to resolve subglacial topography at unprecedented levels of spatial detail and precision, thereby enabling even greater levels of insight into a wide range of subglacial landforms and processes.

A necessity for large-scale automated mapping exercises is the definition of simple yet sufficiently precise methods that can delimit and classify landforms correctly in a particular terrain (e.g. Saha et al., 2011). Glacial overdeepenings present a considerable challenge in this respect because enclosed-depressions can be representative of processes other than direct glacial erosion, though large tectonic basins (e.g.Wilkes subglacial basin) are easily excluded and smaller tectonic basins, such as the Vostok basin in East Antarctica, are relatively rare. Consequently, and given poor knowledge of subglacial geology for the large ice sheets, the implementation of methods for automated exclusion of all non-glacial basins is not considered efficient. Depressions also occur that are artefacts introduced during interpolation of raw bed-elevation measurements, for which automated exclusion methods are possible, but these are not without problems (see below). An overriding concern, however, is how to define overdeepenings as mappable landforms. For purposes of understanding overdeepening evolution, which is likely to occur over timescales longer than a single glacial cycle, identification and mapping of overdeepenings as 'subaerial' enclosed-depressions is perspicacious. It therefore must be stressed that not all overdeepenings mapped using our methods are 'enclosed-depressions' in terms of the subglacial hydraulic gradient, and a different mapping approach may be required where it is necessary to understand overdeepening influence on contemporary ice-bed conditions and processes. Consequently, a glaciologically meaningful and robust definition of the term 'overdeepening' remains elusive, but is never more urgently needed to stimulate empirical research and model testing. Further consideration also needs to be given to the significance of 'nested' depressions for mapping of overdeepenings and understanding of their origin and evolution.

The timescale of overdeepening formation also presents particular challenges. Changes in ice-sheet configuration associated with glacial cycles and shorter-term climatic variations affect flow patterns and hydrological gradients, meaning overdeepening form may reflect a complex erosion history and may even reflect erosion during ice-sheet configurations that are discordant with those present today. This is particularly to be expected given modelling evidence that indicates rapid landscape evolution during initial glacial cycles, followed by relative landscape stability (e.g. Jamieson et al., 2010; Kessler et al., 2008). Consequently, recent climatic changes may mean that present overdeepening morphologies are not necessarily in equilibrium with relevant driving factors. Further, for Antarctica in particular, characteristically slow rates of subglacial erosion and sediment transport under ice sheets may result in overdeepening morphologies remaining in permanent disequilibrium with these factors. The strict quality criteria that are recommended and applied in this study, in particular the requirement that depressions are elongated in the direction of current ice flow, are intended to focus analysis on that portion of the dataset that is most likely to comprise overdeepenings that are in balance with the glaciological factors that drive erosion and sediment transportation. Nevertheless, as demonstrated in the example study of the relationship

between overdeepening ER and ice velocity, the likely timescales of overdeepening formation are likely to weaken the potential to develop process-based insights using empirical landform data from contemporary ice sheet settings.

6.2 Source data limitations and methodological recommendations

The quality of mapping results and the process-based insights that can be obtained using associated empirical data are dependent on the resolution and quality of available bed topography data. Datasets that are presently available for the whole of the Greenland and Antarctic ice sheets have important limitations, meaning that, when applied to such datasets, the outcomes of the mapping approaches, including the example study above, require careful evaluation and analysis.

A major limitation, particularly for Bedmap2, is the absolute uncertainty of large swathes of the subglacial topography. For some areas of the East Antarctic interior, absolute bed-elevation uncertainties range up to 1,008 m (Fretwell et al., 2013). Conversely, for the most recent DEM covering Greenland (Bamber et al., 2013), some of the largest errors occur in the mountainous coastal fjord regions where extrapolation, rather than interpolation, has been required to resolve bed elevations. These fjord regions are prime locations for overdeepening development, where topographic confinement dominates the configuration of outflowing ice. Nevertheless, comparison of features mapped from large-scale datasets with those from higher resolution subset domains (e.g. Fig. 10) reveals an encouraging level of consistency. Notably, for the Byrd Glacier depression (Fig. 10 C–D), long-profile form (Fig. 10E) is resolved relatively well by Bedmap2 in comparison to the higher-resolution product, with only minor differences in maximum absolute depth. On the other hand, the size, form and number of smaller depressions in the Byrd Catchment (Fig. 10C-D) is very much influenced by flightline density (Fig. 10A–B), and artefact depressions created at flightline intersections by the interpolation method (i.e. kriging) are evident at both dataset resolutions. Quality control criteria that remove such depressions, as applied in the example study above, are therefore necessary regardless of resolution. Acquisition of even higher-resolution datasets using novel extrapolation approaches (e.g. Morlighem et al., 2014) offers the potential to further understand and improve bed-elevation uncertainties, but kriging is still required where ice flow velocities are low and empirical ice thickness measurements are scarce. The scarcity of empirical measurements across large areas of the present ice sheets means therefore that significant areas of uncertainty will remain.

Morphological studies of subglacial phenomena thus require strict appreciation of the uncertainties inherent within the source datasets. The application of multiple quality criteria to mapped results, such as minimum flightline density, is viewed as essential to minimise the introduction of unreliable or spurious data. As such, the limitations of existing subglacial topography datasets

564 mean that the subglacial area that is suitable for landform analyses of the kind presented here is
565 only a fraction of the total area (e.g. only 36% of the grounded Antarctic bed is constrained by
566 measured data at a 5 km resolution in Bedmap2). Formerly glaciated areas on the adjacent
567 continental shelves offer potential to greatly increase the mappable area: for example, studies in
568 Antarctica show that glacial and post-glacial sedimentation in offshore areas may be only 4-5 m
569 thick (e.g. Dowdeswell et al., 2004) and is therefore well below the minimum bed elevation
570 uncertainty in subglacial areas. However, detailed sediment thickness data for offshore areas is
571 available for only limited areas, and there is limited potential to relate landform location and
572 morphology to ice sheet parameters. In addition, fjord depths are poorly constrained along much of
573 the Greenland coastline, meaning subglacial and offshore topographies are often mismatched by as
574 much as several hundred metres (Bamber et al., 2013). Further strategic data collection is therefore
575 required to address areas of uncertainty, both in the interiors of ice sheets and at present ice-sheet
576 margins.

577 # 7. Conclusions

578 Motivated by the release of comprehensive, 1 km gridded datasets detailing the subglacial
579 topography of Greenland and Antarctica (Bamber et al., 2013; Fretwell et al., 2013), automated
580 methods have been explored for mapping glacial overdeepenings and the extraction of metrics the
581 describe their form. Hydrological tools and terrain filtering fail to adequately capture the complex
582 morphologies of overdeepenings, primarily because terrain filtering lacks precise thresholds
583 required for delimiting enclosed-depression boundaries and because both methods lack the ability
584 to resolve depression nesting. A novel rule-based GIS methodology has therefore been proposed
585 that quantitatively tracks changes in the length of closed-contours from initial points of elevation
586 minima. This method provides consistent, morphologically based mapping results and is
587 computationally efficient at ice sheet scales. Its application is therefore not dependent on a
588 particular bed-dataset resolution, requires no abstract threshold parameters to be defined, and is
589 unlikely to be restricted or compromised by anticipated improvements in dataset quality and detail.
590 However, difficulties associated with the acquisition of detailed and accurate subglacial
591 topographies means that mapped features require robust scrutiny. A suite of simple quality control
592 criteria that are applicable to the 1 km gridded datasets for Greenland and Antarctica have
593 therefore been described that may be adapted according to the nature of the bed-topography
594 dataset or the specific focus of a given study.

595 The ability to relate overdeepening characteristics to present ice sheet characteristics means our
596 approach provides significant potential to gain insight into critical ice-bed processes, including
597 those that influence the location, timescale and nature of overdeepening formation, and the co-

598 evolution of ice sheets and their subglacial topographies. To demonstrate this potential, we have
599 conducted a preliminary analysis of a proposed relationship between overdeepening elongation
600 and ice-flow velocity using data for a large sample of depressions mapped beneath the Antarctic
601 and Greenland ice sheets. Although strict quality criteria were applied to avoid the inclusion of
602 spurious depressions arising from DEM artefacts, the limitations of present datasets and the
603 simplicity of our approach means that strong statistical relationships cannot be expected. Dataset
604 limitations are associated with the density and accuracy of empirical bed-elevation measurements,
605 meaning the level of insight that can be acquired is dependent upon the quality of the metrics that
606 such data permit. Limitations associated with our approach include unidentified influences on
607 overdeepening length or width (notably valley width), the long timescale of overdeepening
608 formation relative to that of climatic changes that influence present ice velocities, and our
609 assumption that erosion processes scale linearly with ice velocity and do not depend on other
610 factors (cf. the likely influence on quarrying rates of subglacial water pressure variation; e.g.
611 Hooke, 1991; Egholm et al., 2012). More importantly, the significance of reverse bed-slopes in
612 glacial systems indicates that the introduction of overdeepenings into ice sheet beds is itself
613 expected to modulate ice velocities, meaning overdeepening metrics may demonstrate non-linear
614 relationships with ice velocity that reflect a more fundamental process of ice sheet co-evolution
615 with the underlying topography. Nevertheless, qualified relationships between overdeepening ER
616 and ice velocity were found and, given anticipated improvements in dataset accuracy and
617 resolution, further work is recommended to better resolve them.

618 This work demonstrates that the exploration of subglacial landform morphology and evolution
619 within an empirical glaciological framework has potential to provide valuable insights for the
620 geomorphology and numerical ice sheet modelling communities. Difficulties involved in acquiring
621 detailed and accurate subglacial topographies means the production of comprehensive datasets
622 requires interpolation and extrapolation of empirical measurements and their associated
623 uncertainties. Consequently, mapping and analysis of even the largest subglacial landforms,
624 including troughs, cirques and overdeepenings, will be an exercise marked with varying aspects of
625 uncertainty that requires strict quality control procedures and close scrutiny of mapping and metric
626 outputs. Nevertheless, anticipated improvements in the accuracy and resolution of bed-topography
627 datasets, including novel extrapolation methods that utilise surface ice velocities, will reduce the
628 need for quality control procedures and achieve convergence of measured landform attributes on
629 'true' values that will facilitate increasingly robust insights from empirical data.

630 **Acknowledgements**

631 This work was carried out with funding from the National Cooperative for the Disposal of
632 Radioactive Waste (NAGRA) (Ref: Nagra Aktennotiz AN 14-146). We acknowledge the use of

633 data and/or data products from CReSIS generated with support from NSF grant ANT-0424589 and
634 NASA Operation IceBridge grant NNX13AD53A. Discussions with Andrew Sole and Jeremy Ely
635 helped to advance ideas produced in this study, and are gratefully acknowledged.

636 **References**

637 Alley, R.B., Lawson, D.E., Larson, G.J., Evenson, E.B., Baker, G.S., 2003. Stabilizing feedbacks
638 in glacier-bed erosion. Nature 424, 758–60. doi:10.1038/nature01839

639 Arnold, N., 2010. A new approach for dealing with depressions in digital elevation models when
640 calculating flow accumulation values. Prog. Phys. Geogr. 34, 781–809.
641 doi:10.1177/0309133310384542

642 Bamber, J.L., Griggs, J.A., Hurkmans, R.T.W.L., Dowdeswell, J.A., Gogineni, S.P., Howat, I.,
643 Mouginot, J., Paden, J., Palmer, S., Rignot, E., Steinhage, D., 2013. A new bed elevation dataset
644 for Greenland. Cryosph. 7, 499–510. doi:10.5194/tc-7-499-2013

645 Brenning, A., 2009. Benchmarking classifiers to optimally integrate terrain analysis and
646 multispectral remote sensing in automatic rock glacier detection. Remote Sens. Environ. 113, 239–
647 247. DOI: 10.1016/j.rse.2008.09.005

648 Clark, C.D., 1993. Mega-scale glacial lineations and cross-cutting ice-flow landforms. Earth Surf.
649 Process. Landforms 18, 1–29. DOI: 10.1002/esp.3290180102

650 Clark, C.D., Hughes, A.L.C., Greenwood, S.L., Spagnolo, M., Ng, F.S.L., 2009. Size and shape
651 characteristics of drumlins, derived from a large sample, and associated scaling laws. Quat. Sci.
652 Rev. 28, 677–692. doi:10.1016/j.quascirev.2008.08.035

653 Clarke, G.K.C., 2005. Subglacial Processes. Annu. Rev. Earth Planet. Sci. 33, 247–276.
654 doi:10.1146/annurev.earth.33.092203.122621

655 Cook, S.J., Swift, D.A., 2012. Subglacial basins: Their origin and importance in glacial systems
656 and landscapes. Earth-Science Rev. 115, 332–372. DOI: 10.1016/j.earscirev.2012.09.009

657 Dowdeswell, J.A., Cofaigh, C.Ó., Pudsey, C.J., 2004. Thickness and extent of the subglacial till
658 layer beneath an Antarctic paleo–ice stream. Geology 32, 13. doi:10.1130/G19864.1

659 Drăguţ, L., Blaschke, T., 2006. Automated classification of landform elements using object-based
660 image analysis. Geomorphology 81, 330–344. DOI: 10.1016/j.geomorph.2006.04.013

661 Dunlop, P., Clark, C.D., 2006. The morphological characteristics of ribbed moraine. Quat. Sci.
662 Rev. 25, 1668–1691. doi:10.1016/j.quascirev.2006.01.002

663 Egholm, D.L., Pedersen, V.K., Knudsen, M.F., Larsen, N.K., 2012. On the importance of higher
664 order ice dynamics for glacial landscape evolution. Geomorphology 141-142, 67–80.
665 doi:10.1016/j.geomorph.2011.12.020

666 Evans, D.J.A., 2009. Controlled moraines: origins, characteristics and palaeoglaciological
667 implications. Quat. Sci. Rev. 28, 183–208. DOI: 10.1016/j.quascirev.2008.10.024

668 Evans, I.S., 1980. An integrated system of terrain analysis and slope mapping. Zeitschrift fur
669 Geomorphol. Suppl-Bd 3, 274–295.

670 Fountain, A.G., Walder, J.S., 1998. Water flow through temperate glaciers. Rev. Geophys. 36,
671 299. doi:10.1029/97RG03579

672 Fretwell, P., Pritchard, H.D., Vaughan, D.G., Bamber, J.L., Barrand, N.E., Bell, R., Bianchi, C.,
673 Bingham, R.G., Blankenship, D.D., Casassa, G., Catania, G., Callens, D., Conway, H., Cook, A.J.,
674 Corr, H.F.J., Damaske, D., Damm, V., Ferraccioli, F., Forsberg, R., Fujita, S., Gim, Y., Gogineni,
675 P., Griggs, J.A., Hindmarsh, R.C.A., Holmlund, P., Holt, J.W., Jacobel, R.W., Jenkins, A., Jokat,
676 W., Jordan, T., King, E.C., Kohler, J., Krabill, W., Riger-Kusk, M., Langley, K.A., Leitchenkov,
677 G., Leuschen, C., Luyendyk, B.P., Matsuoka, K., Mouginot, J., Nitsche, F.O., Nogi, Y., Nost,
678 O.A., Popov, S. V., Rignot, E., Rippin, D.M., Rivera, A., Roberts, J., Ross, N., Siegert, M.J.,
679 Smith, A.M., Steinhage, D., Studinger, M., Sun, B., Tinto, B.K., Welch, B.C., Wilson, D., Young,
680 D.A., Xiangbin, C., Zirizzotti, A., 2013. Bedmap2: improved ice bed, surface and thickness
681 datasets for Antarctica. Cryosph. 7, 375–393. doi:10.5194/tc-7-375-2013

682 Glasser, N.F., Bennett, M.R., 2004. Glacial erosional landforms: origins and significance for
683 palaeoglaciology. Prog. Phys. Geogr. 28, 43–75. doi:10.1191/0309133304pp401ra

684 Greenwood, S.L., Clark, C.D., 2009. Reconstructing the last Irish Ice Sheet 2: a
685 geomorphologically-driven model of ice sheet growth, retreat and dynamics. Quat. Sci. Rev. 28,
686 3101–3123. doi:10.1016/j.quascirev.2009.09.014

687 Hansen, L., Beylich, A., Burki, V., Eilersten, R.S., Fredin, O., Larsen, E., Lysså, A., Nesje, A.,
688 Stalsberg, K., Tønnesen, J.F., 2009. Stratigraphic architecture and infill history of a deglaciated
689 bedrock valley based on georadar, seismic profiling and drilling. Sedimentology 56, 1751–1773.
690 doi:10.1111/j.1365-3091.2009.01056.x

691 Heidenreich, C., 1964. Some observations on the shape of drumlins. Can. Geogr. 8, 101–107.
692 doi:10.1111/j.1541-0064.1964.tb00591.x

693 Herman, F., Beaud, F., Champagnac, J.D., Lemieux, J.M., Sternai, P., 2011. Glacial hydrology and
694 erosion patterns: a mechanism for carving glacial valleys. Earth Planet. Sci. Lett. 310, 498–508.
695 DOI: 10.1016/j.epsl.2011.08.022

696 Hooke, R.L., 1991. Positive feedbacks associated with erosion of glacial cirques and
697 overdeepenings. Geol. Soc. Am. Bull. 103, 1104–1108. doi: 10.1130/0016-
698 7606(1991)103<1104:PFAWEO>2.3.CO;2

699 Huuse, M., 2000. Overdeepened Quaternary valleys in the eastern Danish North Sea: morphology
700 and origin. Quat. Sci. Rev. 19, 1233–1253. doi:10.1016/S0277-3791(99)00103-1

701 Huybrechts, P., 1993. Glaciological modelling of the late Cenozoic East Antarctic ice sheet:
702 Stability or dynamism? Geogr. Ann. A 75, 221-238. DOI: 10.2307/521202

703 Jakobsson, M., Mayer, L., Coakley, B., Dowdeswell, J.A., Forbes, S., Fridman, B., Hodnesdal, H.,
704 Noormets, R., Pedersen, R., Rebesco, M., Schenke, H.W., Zarayskaya, Y., Accettella, D.,
705 Armstrong, A., Anderson, R.M., Bienhoff, P., Camerlenghi, A., Church, I., Edwards, M., Gardner,
706 J. V., Hall, J.K., Hell, B., Hestvik, O., Kristoffersen, Y., Marcussen, C., Mohammad, R., Mosher,
707 D., Nghiem, S. V., Pedrosa, M.T., Travaglini, P.G., Weatherall, P., 2012. The International
708 Bathymetric Chart of the Arctic Ocean (IBCAO) Version 3.0. Geophys. Res. Lett. 39, L12609.
709 doi:10.1029/2012GL052219

710 Jamieson, S.S.R., Sugden, D.E., Hulton, N.R.J., 2010. The evolution of the subglacial landscape of
711 Antarctica. Earth Planet. Sci. Lett. 293, 1–27. doi:10.1016/j.epsl.2010.02.012

712 Joughin, I.B., Smith, B., Howat, I., Scambos, T.A., 2010a. MEaSUREs Greenland Ice Sheet
713 Velocity Map from InSAR Data. National Snow and Ice Data Center., Boulder, Colorado USA.
714 doi:nsidc-0478.001

715 Joughin, I.B., Smith, B.E., Howat, I.M., Scambos, T., Moon, T., 2010b. Greenland flow variability
716 from ice-sheet-wide velocity mapping. J. Glaciol. 56, 415–430. doi:10.3189/002214310792447734

717 Kessler, M.A., Anderson, R.S., Briner, J.P., 2008. Fjord insertion into continental margins driven
718 by topographic steering of ice. Nat. Geosci. 1, 365–369. doi:10.1038/ngeo201

719 King, E.C., Hindmarsh, R.C.A., Stokes, C.R., 2009. Formation of mega-scale glacial lineations
720 observed beneath a West Antarctic ice stream. Nat. Geosci. 2, 585–588. doi:10.1038/ngeo581

721 Klingseisen, B., Metternicht, G., Paulus, G., 2008. Geomorphometric landscape analysis using a
722 semi-automated GIS-approach. Environ. Model. Softw. 23, 109–121. DOI:
723 10.1016/j.envsoft.2007.05.007

724 Leonowicz, A.M., Jenny, B., Hurni, L., 2009. Automatic generation of hypsometric layers for
725 small-scale maps. Comput. Geosci. 35, 2074–2083. doi:10.1016/j.cageo.2008.12.012

726 MacMillan, R.A., Pettapiece, W.W., Nolan, S.C., Goddard, T.W., 2000. A generic procedure for
727 automatically segmenting landforms into landform elements using DEMs, heuristic rules and
728 fuzzy logic. Fuzzy Sets Syst. 113, 81–109. DOI: 10.1016/S0165-0114(99)00014-7

729 Margold, M., Jansson, K.N., Kleman, J., Stroeven, A.P., 2011. Glacial meltwater landforms of
730 central British Columbia. J. Maps 7, 486–506. doi:10.4113/jom.2011.1205

731 Melanson, A., Bell, T., Tarasov, L., 2013. Numerical modelling of subglacial erosion and
732 sediment transport and its application to the North American ice sheets over the Last Glacial cycle.
733 Quat. Sci. Rev. 68, 154–174. doi:10.1016/j.quascirev.2013.02.017

734 Moreau, J., Huuse, M., 2014. Infill of tunnel valleys associated with landward-flowing ice sheets:
735 The missing Middle Pleistocene record of the NW European rivers? Geochemistry, Geophys.
736 Geosystems 15, 1–9. doi:10.1002/2013GC005007

737 Morlighem, M., Rignot, E., Mouginot, J., Seroussi, H., Larour, E., 2014. Deeply incised submarine
738 glacial valleys beneath the Greenland ice sheet. Nat. Geosci. 7, 418–422. doi:10.1038/ngeo2167

739 Nick, F.M., Vieli, A., Howat, I.M., Joughin, I., 2009. Large-scale changes in Greenland outlet
740 glacier dynamics triggered at the terminus. Nat. Geosci. 2, 110–114. doi:10.1038/ngeo394

741 Ó Cofaigh, C., Stokes, C.R., Lian, O.B., Clark, C.D., Tulacyzk, S., 2013. Formation of mega-scale
742 glacial lineations on the Dubawnt Lake Ice Stream bed: 2. Sedimentology and stratigraphy. Quat.
743 Sci. Rev. 77, 210–227. doi:10.1016/j.quascirev.2013.06.028

744 Preusser, F., Reitner, J.M., Schlüchter, C., 2010. Distribution, geometry, age and origin of
745 overdeepened valleys and basins in the Alps and their foreland. Swiss J. Geosci. 103, 407–426.
746 doi:10.1007/s00015-010-0044-y

747 Rignot, E., Mouginot, J., Scheuchl, B., 2011a. MEaSUREs InSAR-Based Antarctica Ice Velocity
748 Map. National Snow and Ice Data Center, Boulder, Colorado USA. doi:nsidc-0484.001

749 Rignot, E., Mouginot, J., Scheuchl, B., 2011b. Ice flow of the Antarctic ice sheet. Science (80-.).
750 333, 1427–30. doi:10.1126/science.1208336

751 Roberts, D.H., Long, A.J., Davies, B.J., Simpson, M.J.R., Schnabel, C., 2010. Ice stream influence
752 on West Greenland Ice Sheet dynamics during the Last Glacial Maximum. J. Quat. Sci. 25, 850–
753 864. doi:10.1002/jqs.1354

754 Saha, K., Wells, N.A., Munro-Stasiuk, M., 2011. An object-oriented approach to automated
755 landform mapping: A case study of drumlins. Comput. Geosci. 37, 1324–1336. DOI:
756 10.1016/j.cageo.2011.04.001

757 Schoof, C., 2007. Ice sheet grounding line dynamics: Steady states, stability, and hysteresis. J.
758 Geophys. Res. 112, F03S28. DOI: 10.1029/2006JF000664

759 Shreve, R.L., 1972. Movement of water in glaciers. J. Glaciol. 11, 205–214.

760 Spagnolo, M., Clark, C.D., Ely, J.C., Stokes, C.R., Anderson, J.B., Andreassen, K., Graham,
761 A.G.C., King, E.C., 2014. Size, shape and spatial arrangement of mega-scale glacial lineations
762 from a large and diverse dataset. Earth Surf. Process. Landforms (in press). doi:10.1002/esp.3532

763 Stokes, C.R., Clark, C.D., 1999. Geomorphological criteria for identifying Pleistocene ice streams.
764 Ann. Glaciol. 28, 67–74. doi:10.3189/172756499781821625

765 Stokes, C.R., Clark, C.D., 2002. Are long subglacial bedforms indicative of fast ice flow? Boreas
766 31, 239–249. doi:10.1111/j.1502-3885.2002.tb01070.x

767 Stokes, C.R., Corner, G.D., Winsborrow, M.C.M., Husum, K., Andreassen, K., 2014.
768 Asynchronous response of marine-terminating outlet glaciers during deglaciation of the
769 Fennoscandian Ice Sheet. Geology 42, 455–458. doi:10.1130/G35299.1

770 Stokes, C.R., Spagnolo, M., Clark, C.D., Ó Cofaigh, C., Lian, O.B., Dunstone, R.B., 2013.
771 Formation of mega-scale glacial lineations on the Dubawnt Lake Ice Stream bed: 1. size, shape
772 and spacing from a large remote sensing dataset. Quat. Sci. Rev. 77, 190–209.
773 doi:10.1016/j.quascirev.2013.06.003

Stumpf, A., Niethhammer, U., Rothmund, S., Mathieu, A., Malet, J.P., Kerle, N., Joswig, M., 2013. Advanced image analysis for automated mapping of landslide surface fissures, in: Margottini, C., Canuti, P., Sassa, K. (Eds.), Landslide Science and Practice Volume 2: Early Warning, Instrumentation and Monitoring. Springer Berlin Heidelberg, Berlin, Heidelberg, pp. 357–363. doi:10.1007/978-3-642-31445-2

Timmermann, R., Le Brocq, A., Deen, T., Domack, E., Dutrieux, P., Galton-Fenzi, B., Hellmer, H., Humbert, A., Jansen, D., Jenkins, A., Lambrecht, A., Makinson, K., Niederjasper, F., Nitsche, F., Nøst, O.A., Smedsrud, L.H., Smith, W.H.F., 2010. A consistent data set of Antarctic ice sheet topography, cavity geometry, and global bathymetry. Earth Syst. Sci. Data 2, 261–273. doi:10.5194/essd-2-261-2010

Van Rensbergen, P., de Batist, M., Beck, C., Chapron, E., 1999. High-resolution seismic stratigraphy of glacial to interglacial fill of a deep glacigenic lake: Lake Le Bourget, Northwestern Alps, France. Sediment. Geol. 128, 99–129. doi:10.1016/S0037-0738(99)00064-0

Vaughan, D.G., Corr, H.F.J., Ferraccioli, F., Frearson, N., O'Hare, A., Mach, D., Holt, J.W., Blankenship, D.D., Morse, D.L., Young, D.A., 2006. New boundary conditions for the West Antarctic ice sheet: Subglacial topography beneath Pine Island Glacier. Geophys. Res. Lett. 33, L09501. doi:10.1029/2005GL025588

Wilson, J.P., Gallant, J.C., 2000. Terrain Analysis, Principles and Applications. John Wiley and Sons, Chichester.

Wood, J., 1996. The geomorphological characterisation of digital elevation models. PhD thesis, University of Leicester. http://www.soi.city.ac.uk/~jwo/phd

Table captions

Table 1: Merits of alternative methods for identification of in- and out-flow points of individual enclosed-depressions. Methods are listed in order of preference.

Figure captions

Figure 1: Examples of overdeepenings beneath contemporary and palaeo ice sheets. (A) Subglacial Lake Ellsworth in East Antarctica (Ross et al., 2011) occupies an overdeepening in a major subglacial trough that cross-cuts the Ellsworth subglacial mountains (figure courtesy Neil Ross). (B) The post-glacial lake Veitastrondvatnet, shown in an oblique aerial view looking due SW,

803 occupies an overdeepening in a sinuous trough confined by the steep topography of the Sognefjord
804 region, Norway. The lake is approximately 17 km long (image: Google Earth). (C) Trough-floor
805 profiles for Jakobshavn Isbrae, Greenland, and Recovery Glacier, Antarctica, derived from bed
806 topography datasets (Bamber et al., 2013; Fretwell et al., 2013) exhibit numerous overdeepenings.
807 Colours highlight reverse-bed slopes: red indicates slope gradients that exceed the supercooling
808 threshold (cf. Alley et al., 2003); blue indicates slope gradients that exceed the ponding threshold
809 (cf. Clarke, 2005). (D) Bathymetry of the bedrock basin occupied by post-glacial Lago Fagnano,
810 Tierra del Fuego, derived from high-resolution single-channel seismic data, showing numerous
811 'child' basins nested within the 'parent' overdeepening (here defined by the present lake margin).
812 Glacial erosion has been conditioned by tectonic processes and the location of numerous faults.
813 MF: Martínez fault; RT: Río Turbio fault; RC: Río Claro fault. Figure from Esteban et al. (2014)
814 courtesy of the author.

815 Figure 2: Cartoon showing the long-profile of a subglacial 'parent' depression containing nested
816 'child' depressions. Various metrics that can be used to describe the form the depression and
817 associated child depressions are defined that can be extracted using GIS-based techniques.

818 Figure 3: Results obtained when applying hydrological tools to identify overdeepenings by means
819 of 'filling' sinks (i.e. enclosed-depressions). The inappropriateness of this method is highlighted
820 by application of the method to two different domains: a smaller 'Byrd' area domain (blue colour
821 scale) and the larger ice sheet domain (red colour scale), of which only a portion is shown (see
822 inset). Some filled sinks in the smaller domain are child depressions (cf. Fig. 2) that are not
823 recognised as distinct features when the method is applied to the ice sheet domain. In addition,
824 some filled sinks in the smaller domain are part of much larger enclosed depressions that are
825 unlikely to be of glacial origin.

826 Figure 4: Identification of areas of overdeepening within the Byrd glacier domain (cf. Fig. 3) using
827 a low-pass, circular (200 km) Gaussian filter. (A) The Bedmap2 DEM filtered using a standard
828 deviation (σ) value of 0.1; (B) the same DEM filtered using a σ value of 25; and (C) negative
829 residuals (A minus B) $\leq$ -450 m, draped over the original Bedmap2 topography.

830 Figure 5: Identification of elevation minima. (A) Initial Bedmap2 DEM; (B) quantitative terrain
831 analysis mask identifying areas of depression-like topography (see text); and (C) points of
832 elevation minima within enclosed depressions (closed contours) contained by the terrain analysis
833 mask.

834 Figure 6: Identification of enclosed-depression perimeters and their nestings using the contour
835 tracking method. (A) Linear transects drawn from each elevation minima intersect with contours.

836 The length change between adjacent contours is calculated to identify abrupt increases in contour
837 length that indicate that a contour is beyond the contour that defines the enclosed-depression
838 perimeter (see text). (B) Parent and child depressions identified using multiple-passes of the
839 contour-tracking algorithm and using a threshold contour-length increase of > 190% to identify the
840 enclosed-depression boundary. (C) Parent and child depressions classified using a top-down
841 approach.

842 Figure 7: Cartoon illustrating the use of the ice-surface elevation data to identify of overdeepening
843 in- and out-flow points for an elongate overdeepening oriented in the direction of ice flow.
844 Topographic focussing of ice flow into the overdeepening means these points are suitable proxies
845 for the principal overdeepening entry and exit points in terms of the greatest ice flux.

846 Figure 8: Identification of overdeepening in- and outflow points using ice surface elevation data
847 (cf. Fig. 7) and overdeepening long-profiles. (A) Ice-surface elevation (coloured scale) draped over
848 the Bedmap2 subglacial topography (grey shading beneath the colour). (B) In- and out-flow points
849 of parent depressions identified from (A) and long profiles, comprising adverse and normal slopes,
850 calculated using a 'least-cost' routing analysis (see text).

851 Figure 9: Depression-shape classification methods and results. (A) Parent depressions enclosed by
852 a polygon representing the smallest rectangle possible by area. (B) A magnified view of the
853 depression boxed in red in (A) showing the bounding rectangle and transects (red lines oriented
854 perpendicular to the least-cost path) used to calculate depression mean width. (C) Example
855 classification output.

856 Figure 10: Comparison of subglacial topography, flightline density, and mapping outputs for
857 Bedmap2 versus a higher resolution dataset (CReSIS; see text) covering a sector of the Byrd
858 Glacier catchment. (A–B) Radar flightline tracks (black) and interpolated subglacial topography
859 (see legend in B). (C–D) Mapping results, showing differences in the shape, size and number of
860 parent and child depressions as a consequence of interpolation of data from contrasting flightline
861 densities to produce datasets with contrasting resolutions. (E) Long-profiles for transect A–A' in
862 (C) and (D).

863 Figure 11: Example application of data on overdeepening form, showing overdeepening
864 elongation ratio versus ice-surface velocity above the overdeepening minima for (A) Antarctica
865 and (B) Greenland. Red points are overdeepenings that are elongated in the direction of ice flow;
866 green points are the subset of these overdeepenings that have been classified as topographically
867 confined. Values for best-fit regression lines show the significance of the regression relationship;
868 R^2 values are ≤ 0.03, reflecting considerable scatter that is discussed in the text.

TABLE 1

Method	Description	Advantage	Disadvantage
Ice-surface based	Minimum and maximum elevations of the ice-sheet surface at the basin edge are used to indicate probable pour points.	* Most reliable indicator of up/down-ice flow, based from relatively easily accessible measurements taken from the ice surface. * Computationally simple.	* Methodology collapses for basins under relatively flat ice shelves, offshore regions where no ice exists, or where basins may have formed under alternative ice-sheet configurations. * Shallow ice-surface relief can produce multiple possible pour points, making discrimination tricky. * Requires full coverage of an additional empirical dataset, leaving it unsuitable for palaeo domains.
Topography based	Mean elevation across a large (>500 km) moving window is used to calculate the likely direction of ice flow across the domain. Further parameters including the range of elevation around the basin edge, and maximum distance from the basin elevation minima, are used to isolate a single pour point.	* Simple technique requiring no additional datasets.	* Local mountain ranges can affect the correct orientation of up- and down-glacier points, depending on the size of the moving window given.
Hydrology based	Flow accumulation calculations and sub-aerial network analyses are used to create a stream network across the domain. Pour points are defined from quantifying the magnitude of flow entering and leaving the basin.	* Most reliable for analysing overdeepenings at the valley-scale glaciation. * Useful for highlighting inherited landforms from time-periods of ice-sheet inception.	* Heavily affected by local watersheds; not suitable for analyses at the ice-sheet scale. * Water flow does not necessarily reflect probable ice-flow.

Figure 01

Click here to download high resolution image

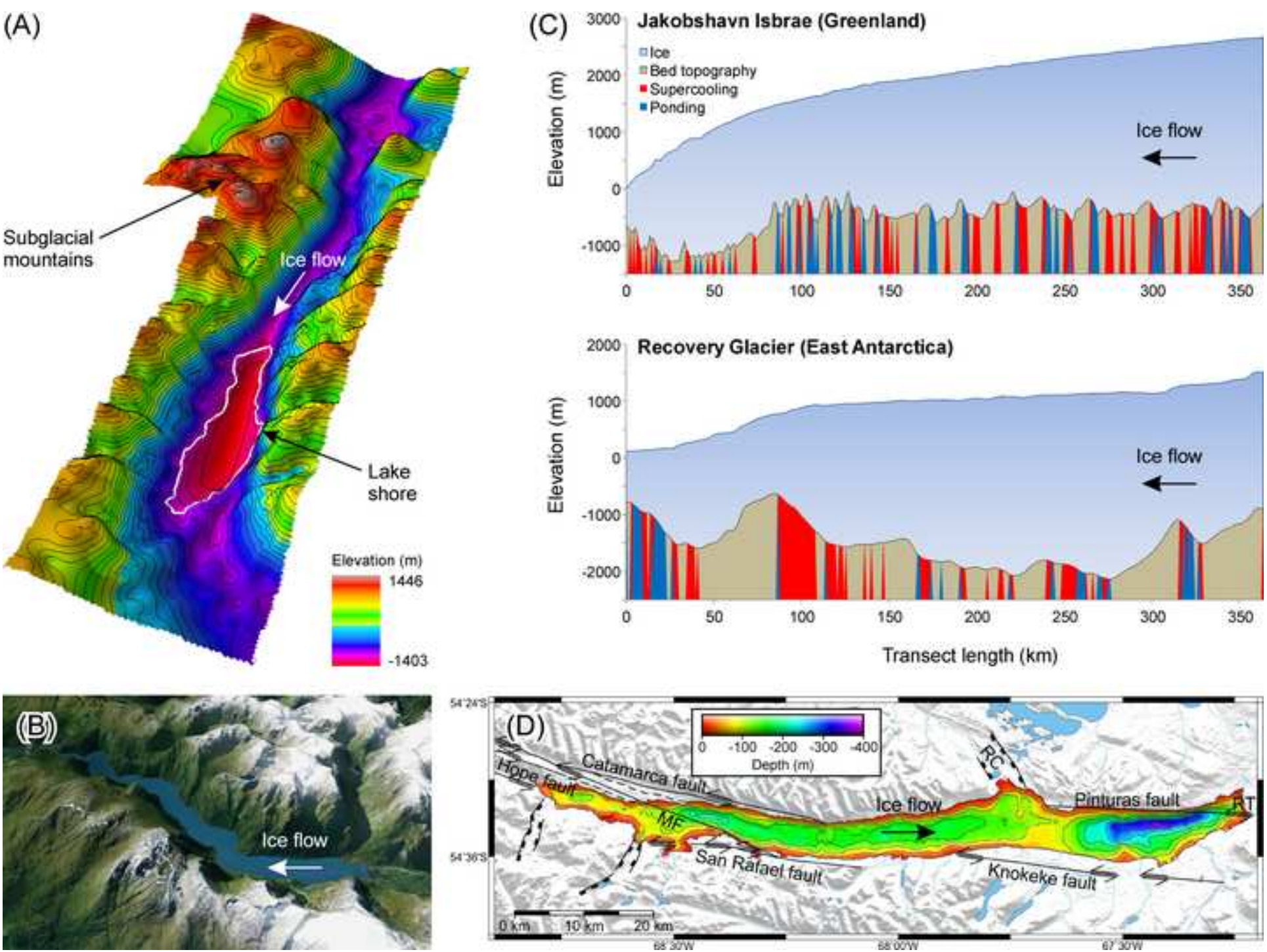

Figure 02

Click here to download high resolution image

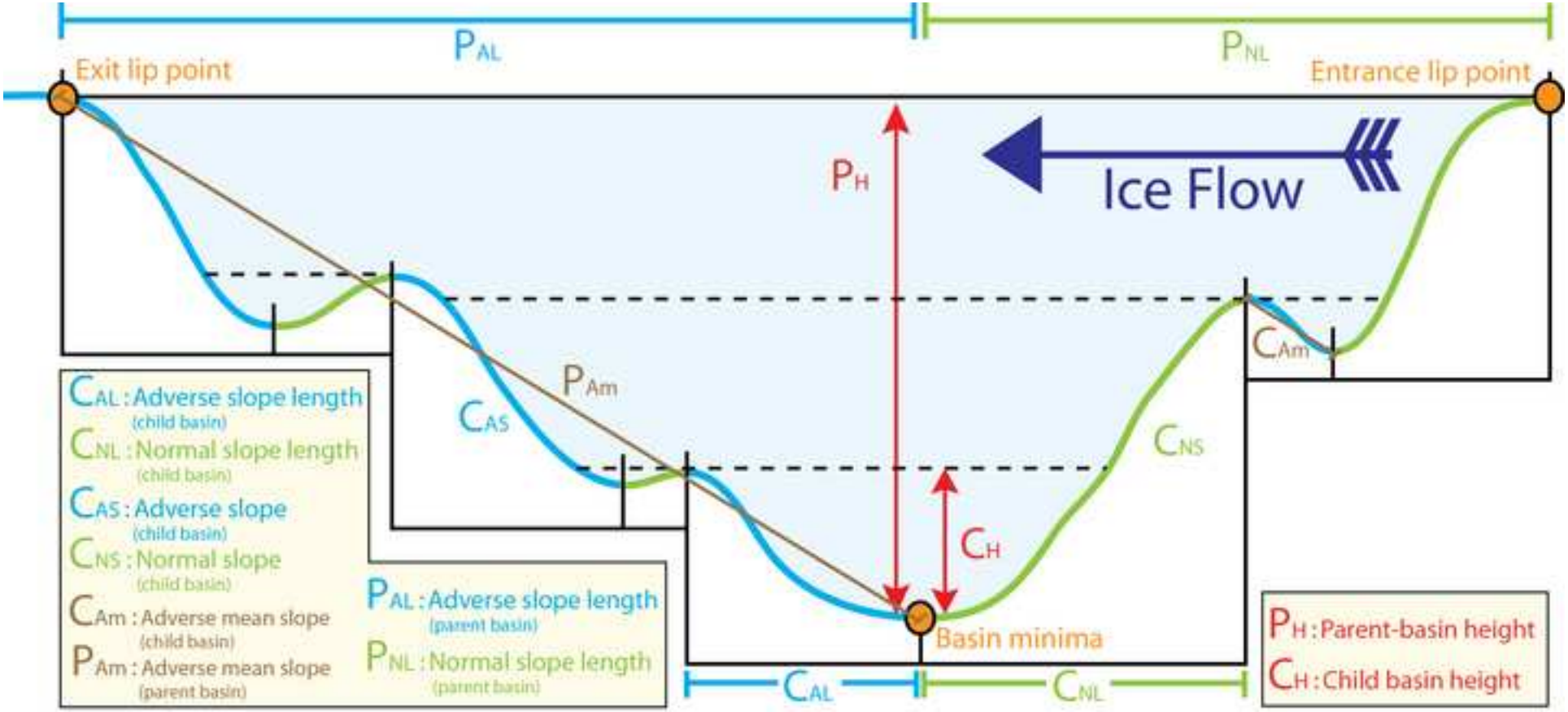

Figure 03

Click here to download high resolution image

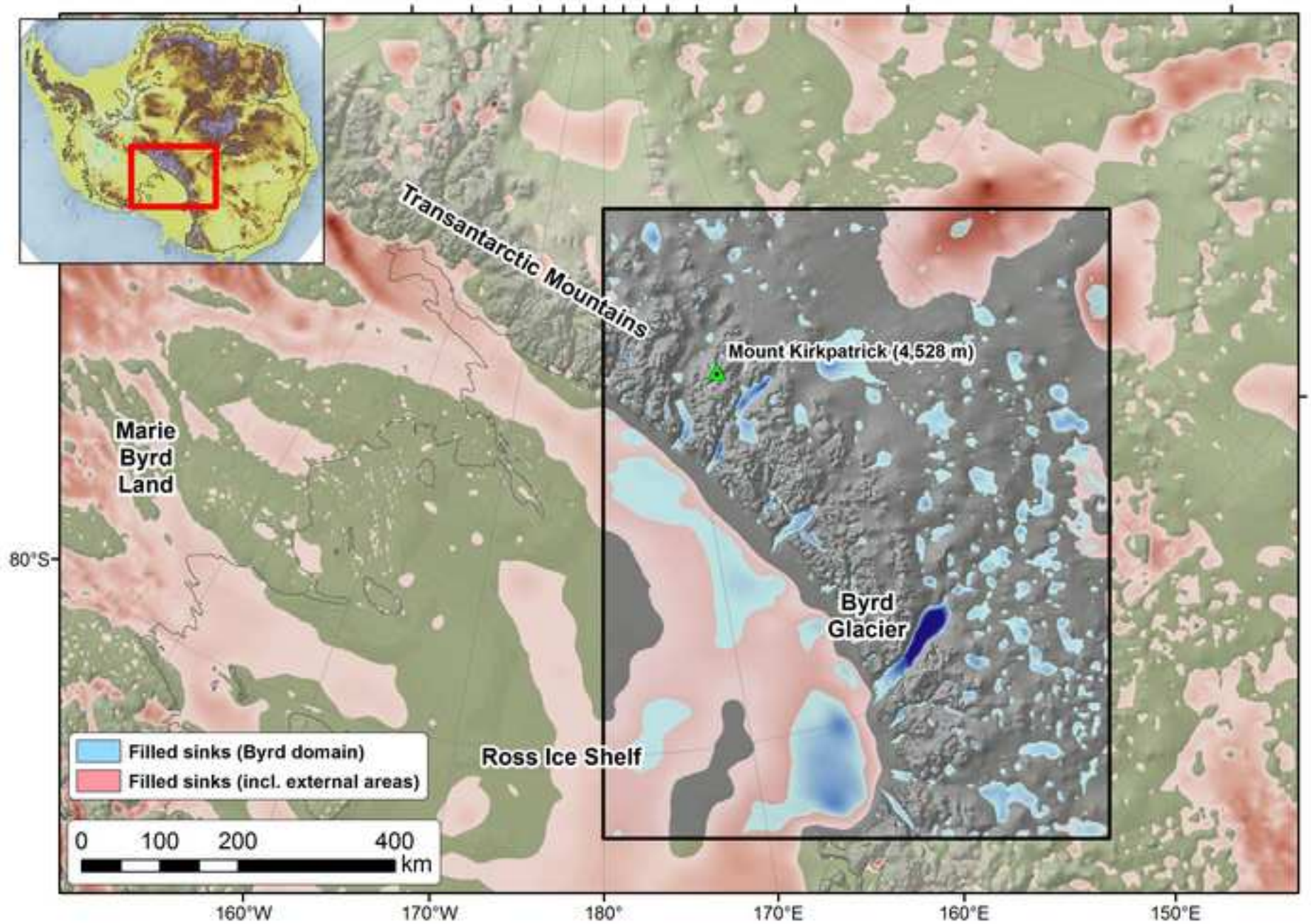

Figure 04

Click here to download high resolution image

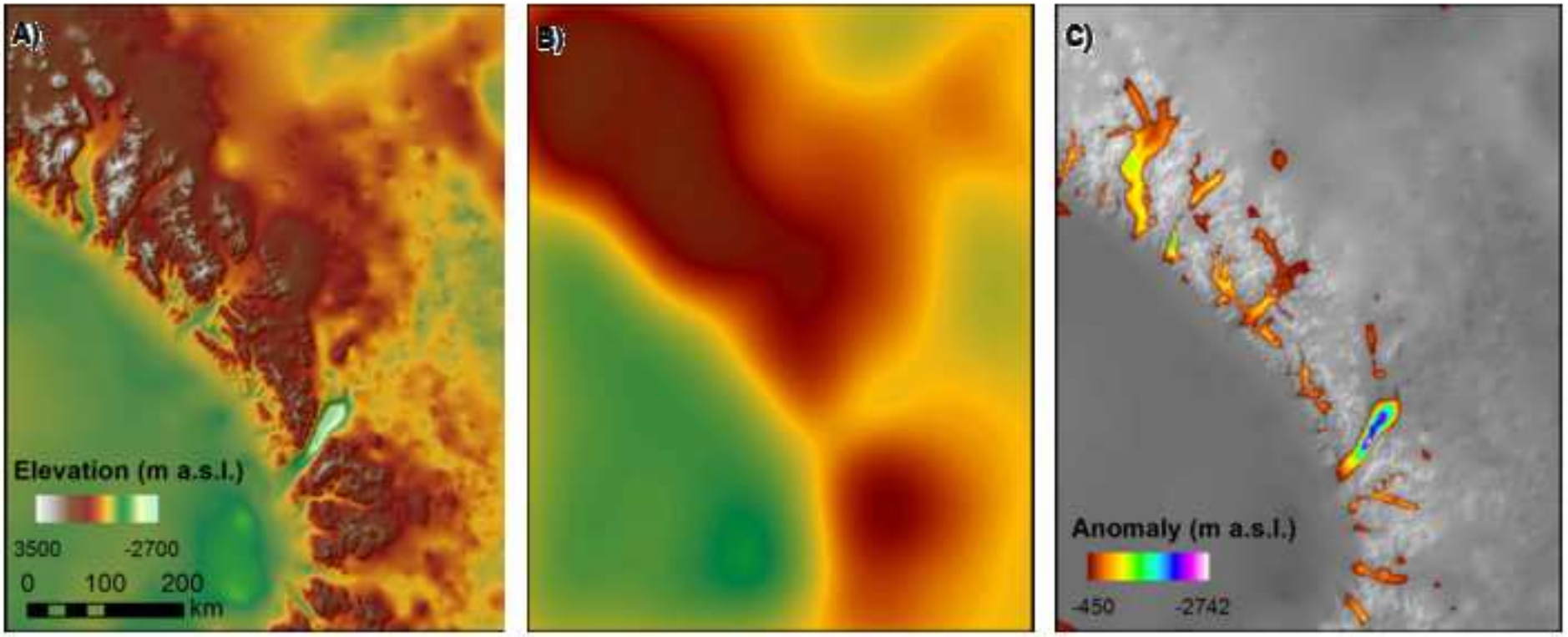

Figure 05

Click here to download high resolution image

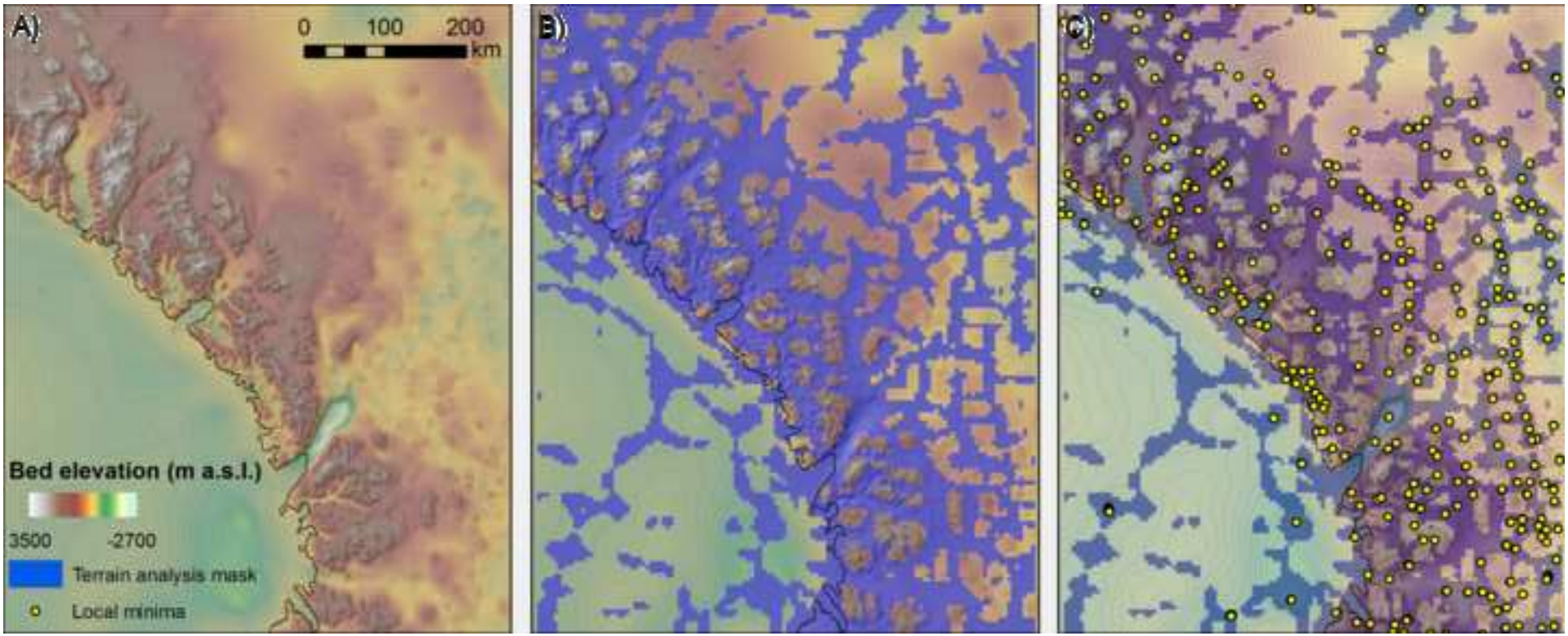

Figure 06

Click here to download high resolution image

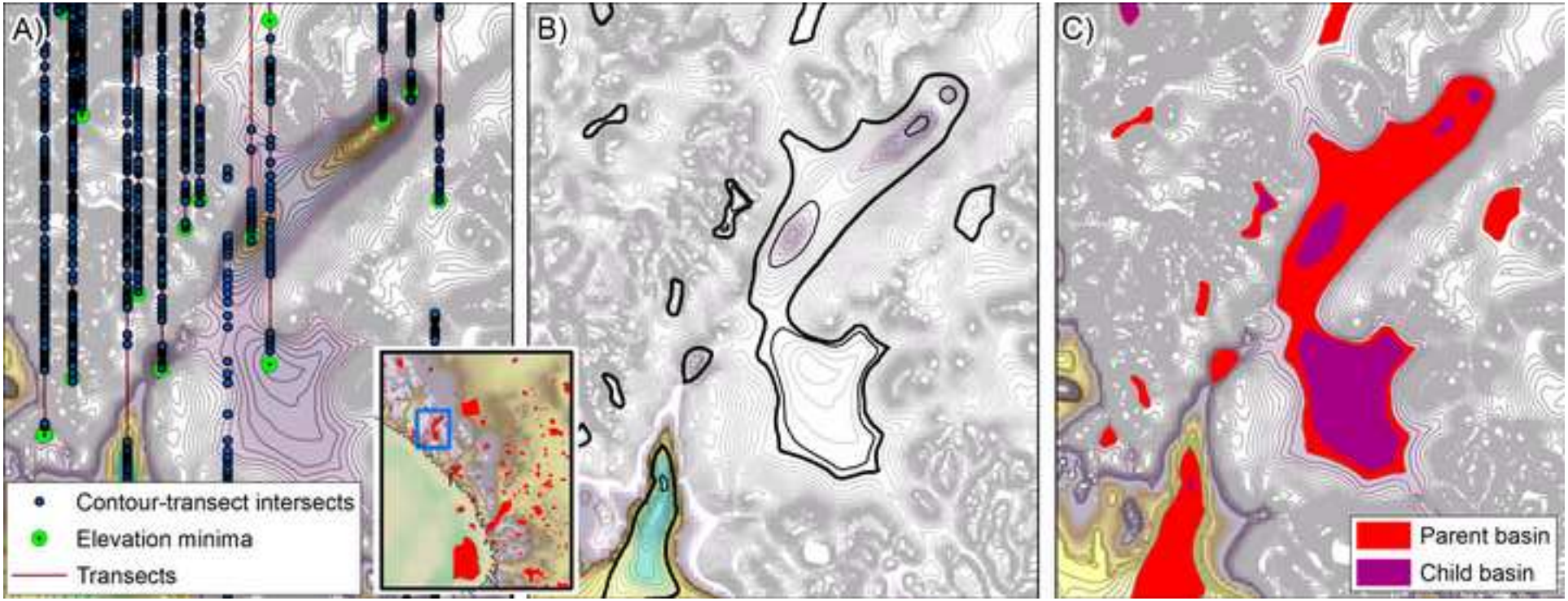

Figure 07
Click here to download high resolution image

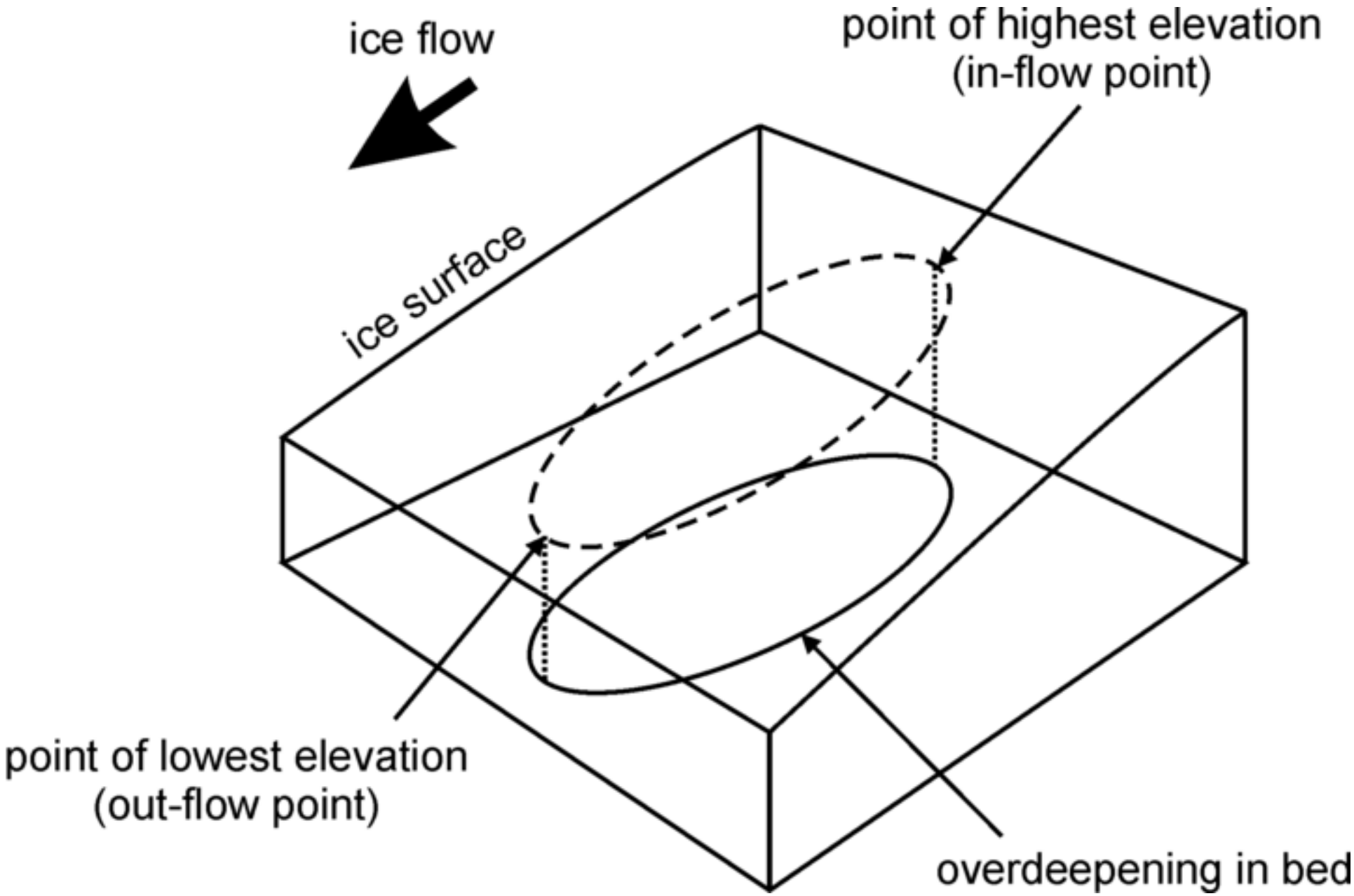

Figure 08

Click here to download high resolution image

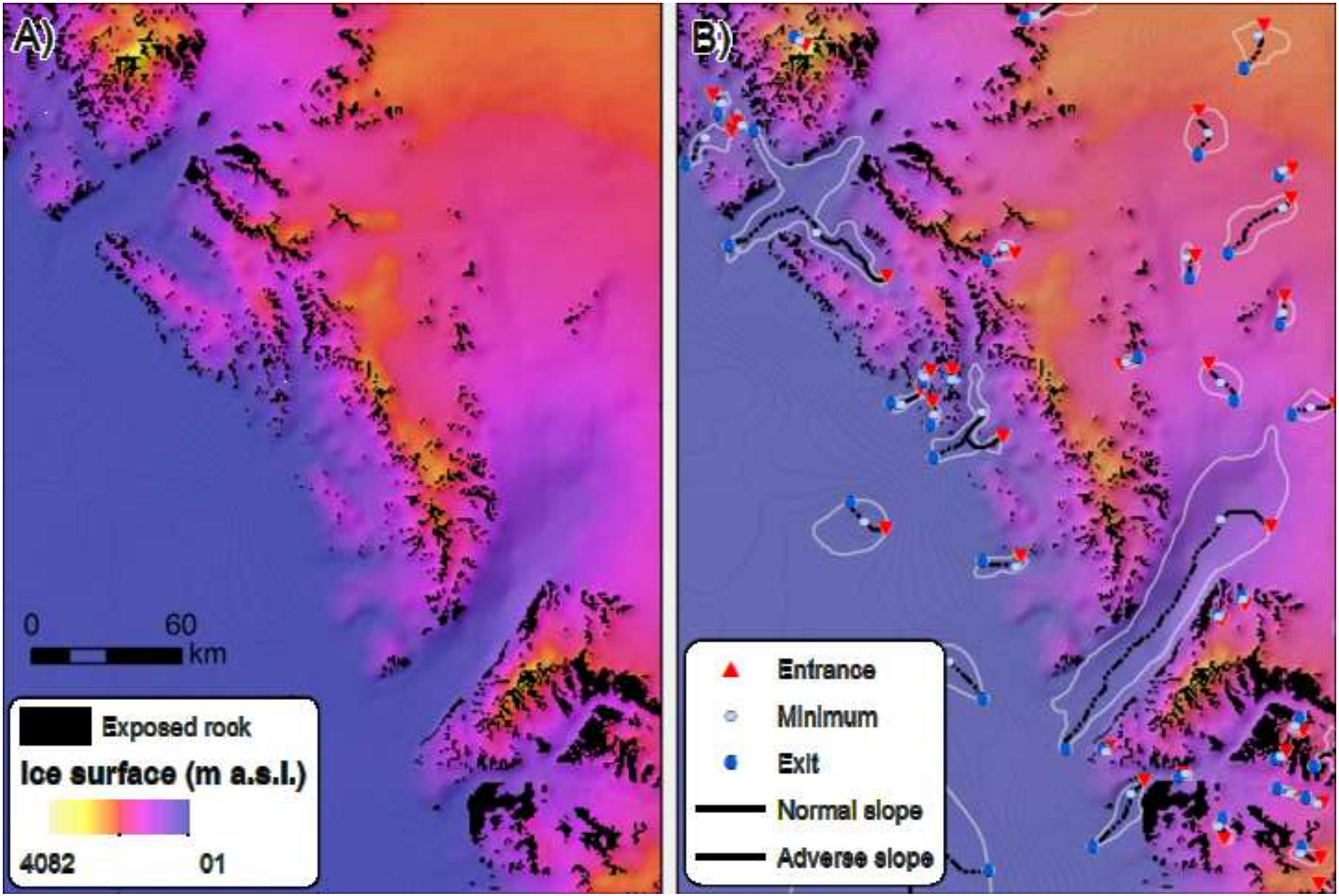

Figure 09

Click here to download high resolution image

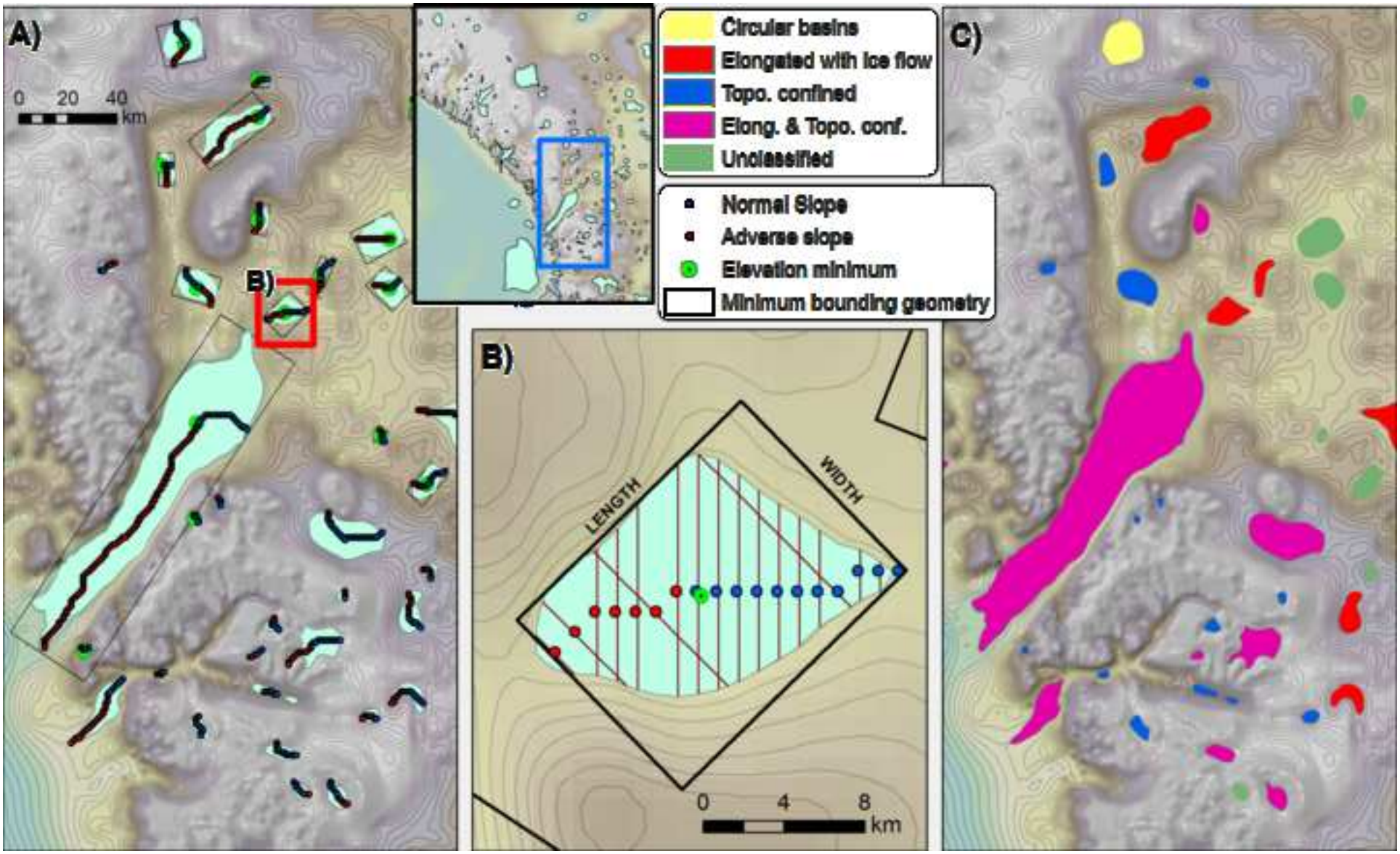

Figure 10

Click here to download high resolution image

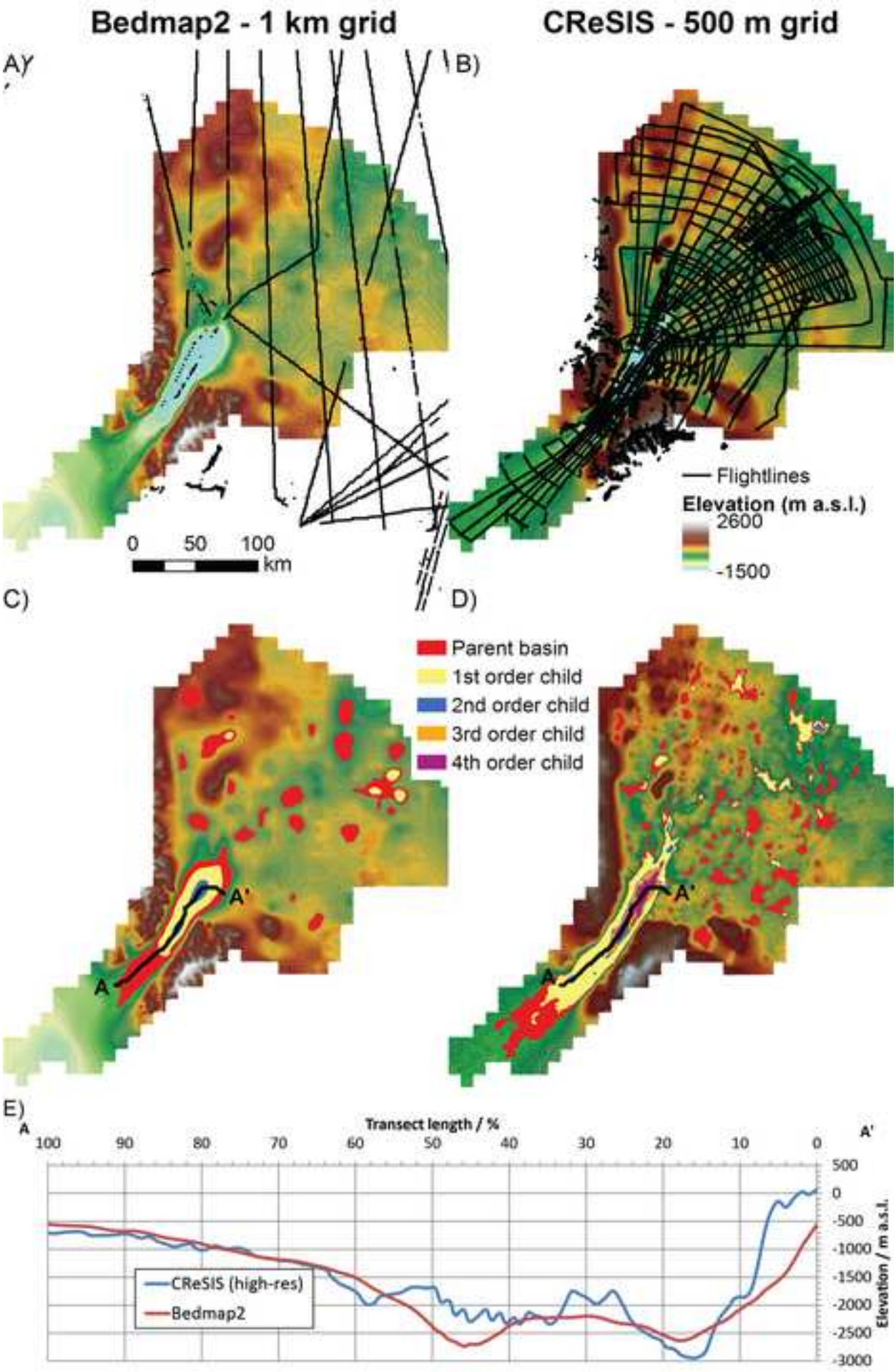

Figure 11

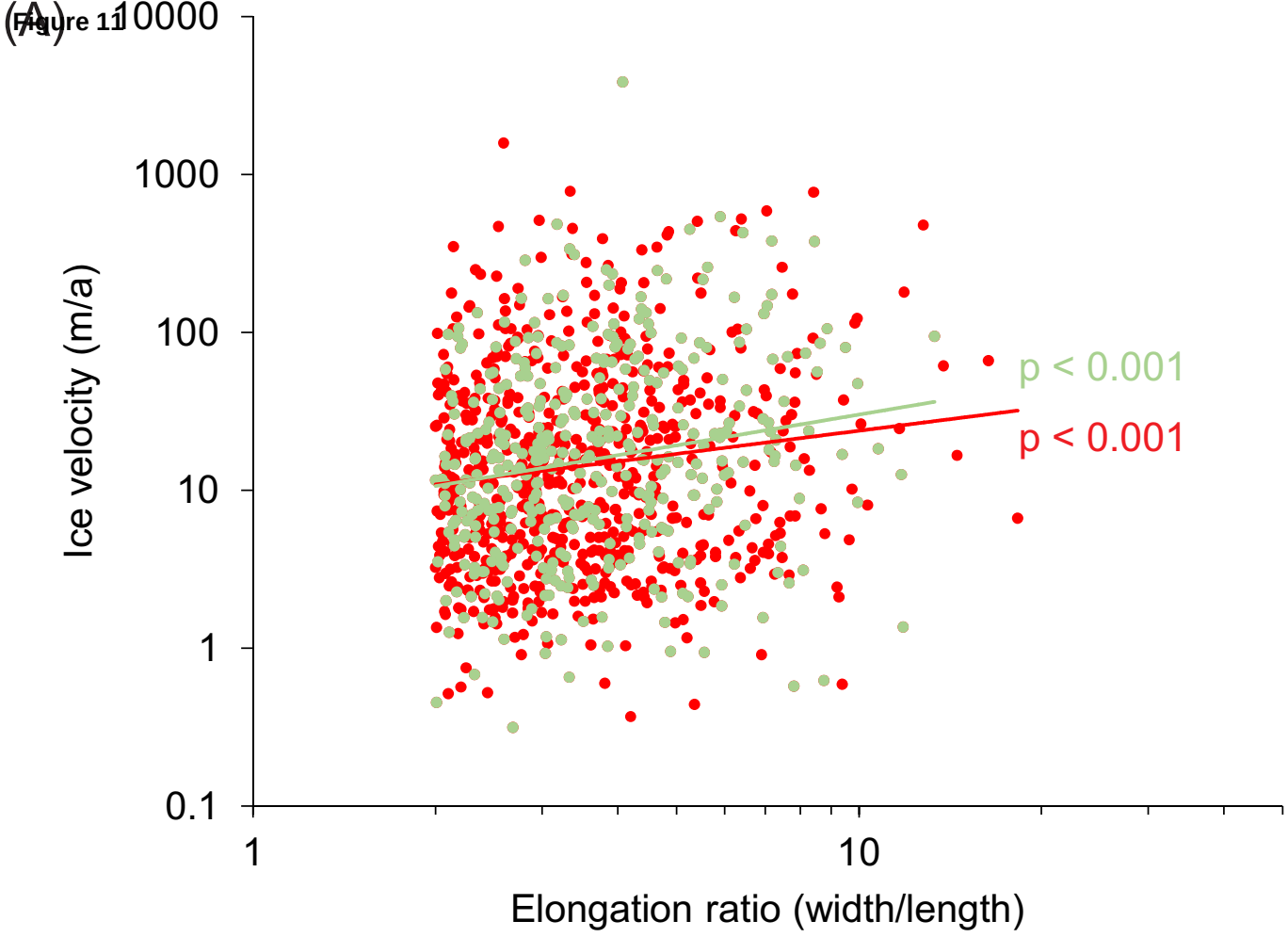
(A)
10000
1000
100
10
1
0.1
Ice velocity (m/a)
p < 0.001
p < 0.001
1
10
Elongation ratio (width/length)

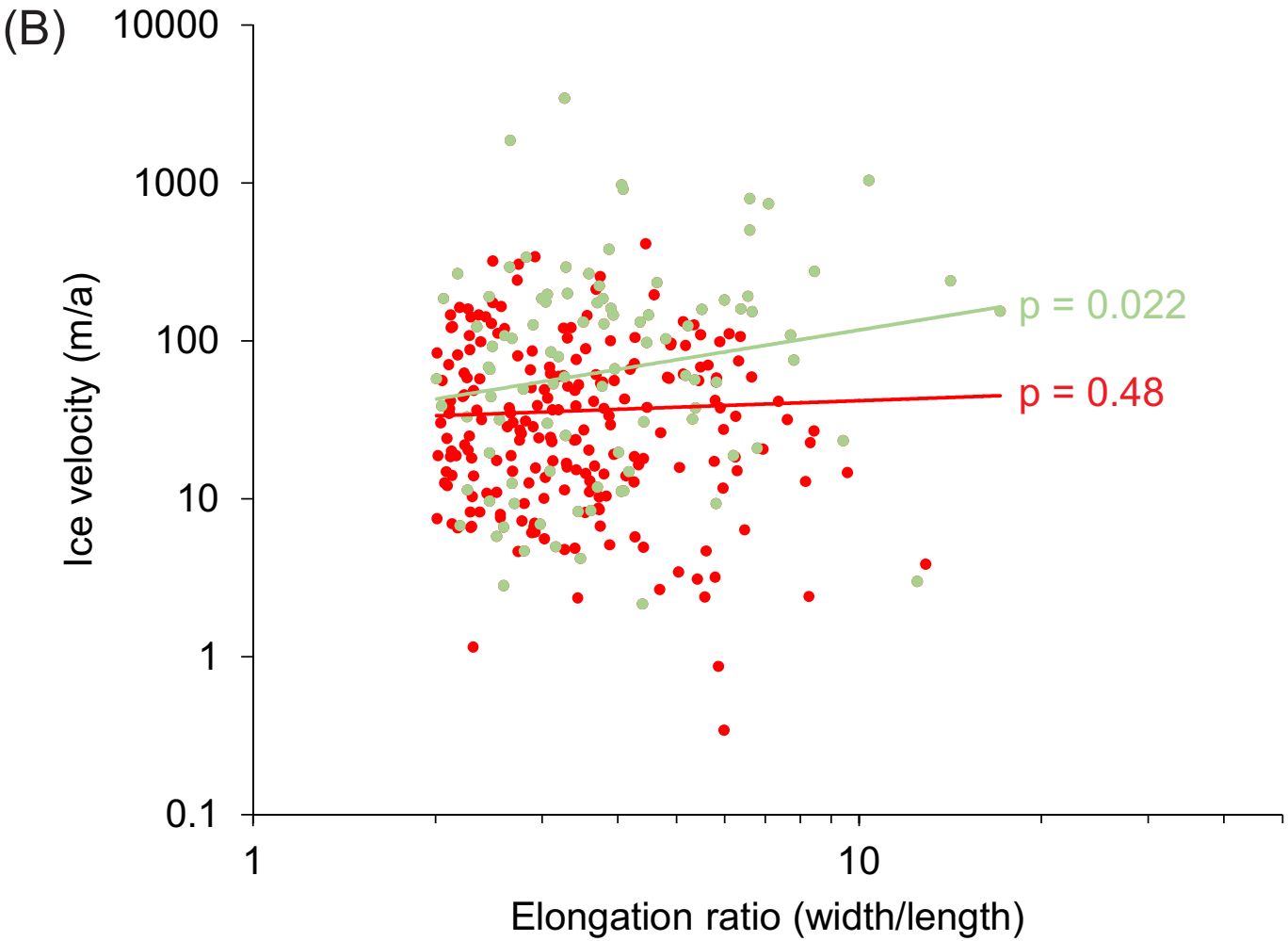
(B)
10000
1000
100
10
1
0.1
Ice velocity (m/a)
p = 0.022
p = 0.48
1
10
Elongation ratio (width/length)